AGU PUBLICATIONS

Radio Science

RESEARCH ARTICLE
10.1002/2015RS005903

Special Section:
Ionospheric Effects Symposium 2015

This article is a companion to *Rino et al.* [2016] doi:10.1002/2015RS005841.

Key Points:
- We extend the phase screen theory of ionospheric scintillation to support two-component spectra
- We validate new theoretical predictions for the behavior of strong scintillations
- We establish the conditions under which a spectral break will influence the scintillation statistics

Correspondence to:
C. S. Carrano,
charles.carrano@bc.edu

Citation:
Carrano, C. S., and C. L. Rino (2016), A theory of scintillation for two-component power law irregularity spectra: Overview and numerical results, *Radio Sci.*, *51*, 789–813, doi:10.1002/2015RS005903.

Received 1 DEC 2015
Accepted 4 MAY 2016
Published online 30 JUN 2016

A theory of scintillation for two-component power law irregularity spectra: Overview and numerical results

Charles S. Carrano[1] and Charles L. Rino[1]

[1]Institute for Scientific Research, Boston College, Chestnut Hill, Massachusetts, USA

Abstract We extend the power law phase screen theory for ionospheric scintillation to account for the case where the refractive index irregularities follow a two-component inverse power law spectrum. The two-component model includes, as special cases, an unmodified power law and a modified power law with spectral break that may assume the role of an outer scale, intermediate break scale, or inner scale. As such, it provides a framework for investigating the effects of a spectral break on the scintillation statistics. Using this spectral model, we solve the fourth moment equation governing intensity variations following propagation through two-dimensional field-aligned irregularities in the ionosphere. A specific normalization is invoked that exploits self-similar properties of the structure to achieve a universal scaling, such that different combinations of perturbation strength, propagation distance, and frequency produce the same results. The numerical algorithm is validated using new theoretical predictions for the behavior of the scintillation index and intensity correlation length under strong scatter conditions. A series of numerical experiments are conducted to investigate the morphologies of the intensity spectrum, scintillation index, and intensity correlation length as functions of the spectral indices and strength of scatter; retrieve phase screen parameters from intensity scintillation observations; explore the relative contributions to the scintillation due to large- and small-scale ionospheric structures; and quantify the conditions under which a general spectral break will influence the scintillation statistics.

1. Introduction

Phase screen theory has been used extensively since the early works of *Booker et al*. [1950] and *Hewish* [1951] to characterize the scintillation of radio waves traversing the ionosphere. One- or two-dimensional phase screens admit analytic representations of the intensity spectral density function (SDF) in terms of combinations of the phase structure function. Early results have been attributed to *Gochelashvily and Shishov* [1971]. The earliest development of the statistical scintillation theory assumed a Gaussian spectral density function. This theory depended on only three parameters, namely, the RMS phase, $<\delta\phi^2>$, a correlation scale, σ, and the Fresnel scale, ρ_F. Various computational methods (generally approximate) were used with results presented as contours of constant S_4 plotted against the dimensionless $(\rho_F/\sigma)^2$ and $<\delta\phi^2>$. The diagrams show strong focusing regions where S_4 exceeds unity [*Singleton*, 1970].

The application of Kolmogorov's theory to atmospheric turbulence was well known at the time scintillation theory was evolving, and it was generally accepted that a power law SDF was a better candidate for ionospheric structure than the more mathematically tractable Gaussian SDF. The first power law computations have been attributed to *Rufenach* [1974]. In these calculations an outer scale wave number was introduced, which played a role similar to σ, but the additional spectral index parameter provided a much broader range of scintillation structure possibilities.

At that time ionospheric researchers assumed that every SDF had a well-defined autocorrelation function that provided an alternative characterization of the structure. However, in the theory of turbulence trend-like departures from strict statistical homogeneity are part of the process. Measurements of turbulent structure are based on models with stationary increments characterized by structure functions. *Rumsey* [1975] was the first to show that robust solutions to the parabolic wave equation can exist even when the structure does not admit an autocorrelation function or even a structure function. He developed a theory of scintillation using an unmodified (unbounded) power law SDF obtained in the limit of an infinitely large outer scale, noting that the solution is "basic to an understanding of propagation in a random medium in the same sense that the plane wave solution is basic to an understanding of wave propagation. Both are idealizations that do not actually occur … Despite this they are basic, because they are simple and exact." *Uscinski et al*. [1981] contrasted the unmodified and modified (with an outer scale) power law models and offered the criticism that the former is physically meaningful only when the observer is so close to the screen that the outer scale cannot be "felt." Later investigations continued to explore the strong scatter behavior associated with propagation through irregularities characterized by a universal Kolmogorov (unmodified) power law [*Gozani*, 1985].

Rino [1979b] noted that an unconstrained inverse power law implies fractal scaling and introduced a normalization which allows the theory of scintillation (at all levels of scattering consistent with the parabolic wave equation) to be completely specified in terms of three parameters, the Fresnel scale, the spectral index, and a universal strength parameter. In effect, a universal scaling was achieved such that different combinations of perturbation strength, propagation distance, and frequency produce the same results. In a series of subsequent papers [*Rino*, 1979b, 1980, 1982; *Rino and Owen*, 1984] he and his colleagues explored the numerical and asymptotic ramifications of this statistical theory of scintillation. Concurrently, *Booker and MajidiAhi* [1981] were also exploring power law phase screen solutions to the problem of strong scintillations, but these authors included both outer and inner scales in their calculations. The ramifications of the Booker and MajidiAhi calculations and analysis were discussed in detail by *Rino and Owen* [1984]. *Forte* [2008, 2012] later employed the theory of Booker and MajidiAhi in a qualitative manner to interpret multifrequency scintillations at auroral [*Forte*, 2008] and equatorial [*Forte*, 2012] latitudes. More recently, *Carrano et al*. [2012] applied the strong scatter theory in the context of an inverse technique to quantitatively infer ionospheric phase screen parameters from measured scintillation time series. In his book, *Rino* [2011] reviewed the parabolic moment equations and discussed the strong scatter behavior of inverse power law phase screen models. In a pair of recent papers, *Zernov and Gherm* [2015] and *Gherm and Zernov* [2015] extended the parabolic moment equations to describe strong scintillations of the wavefield propagating within an inhomogeneous random medium.

Several decades of subsequent scintillation measurements from in situ rocket and satellite beacons have revealed that ionospheric structure exhibits a wide range of inverse power law SDF characteristics. *Shishov* [1974, 1976] developed asymptotic solutions for the case of a two-component (piecewise power law) irregularity spectrum for isotropic three-dimensional irregularities. *Basu et al*. [1983] noted that scintillation at L band was present at Ascension Island only when the intensity decorrelation time at UHF was short. Their reporting of a two-component in situ spectrum (with a spectral break in the inertial range) spawned several studies to reconcile multifrequency scintillation observations. *Franke and Liu* [1983, 1985] advocated the importance of a two-component model in reconciling scintillation observations conducted at multiple frequencies. They also advocated using the intensity correlation length as an important diagnostic in strong scintillation and noted its potential utility in diagnosing the strength of scatter once S_4 has saturated (and thus ceases to vary with further increases in perturbation strength). *Engavale and Bhattacharyya* [2005] simulated the fourth moment of intensity variations numerically for one- and two-component irregularity spectra to investigate the behavior of S_4 and intensity correlation length in the weak and strong scatter regimes. *Forte* [2012] noted the limitations of a one-component spectral model in reconciling scintillations of the Global Positioning System (GPS) satellite signals. To the best of our knowledge, previous modeling efforts involving two-component power law spectra have either been limited to asymptotic results only [*Shishov*, 1974, 1976] or restricted to the particular model $p_1 = 2$, $p_2 = 4$ [*Franke and Liu*, 1983, 1985; *Engavale and Bhattacharyya*, 2005] (for which the structure function takes on a simple form). Two recent papers [*Rino et al*., 2014, 2016] present observations of inverse power law in situ spectra observed with the Planar Langmuir Probe (PLP) on board the Communications/Navigation Outage Forecasting System satellite. The companion study by *Rino et al*. [2016] motivates the need for the present study in the sense that two-component power law spectra are demonstrated to be statistically prominent for highly structured disturbances in premidnight equatorial ionosphere. It also relates the observed in situ spectral characteristics to scintillations observed via ground-based reception of beacon satellite signals.

Rino and Carrano [2013] generalized the statistical theory of scintillation to include a two-component structure model. The generalized theory is completely specified by four parameters: the Fresnel scale, the two spectral indices, and the wave number of the spectral break. The current paper further develops this theory and uses numerical methods to solve the fourth moment equation that is valid for any strength of scatter within the parabolic (paraxial approximation). A forthcoming sequel to this paper employs asymptotic techniques to develop new theoretical predictions for the behavior of the scintillation index and intensity correlation length under asymptotically strong scatter. Recovering the exact solution to the analytic limiting forms validates the numerical calculations. We use the numerical results within the context of a spectral fitting technique to retrieve the model parameters, including scattering strength, low- and high-frequency spectral indices, and the break wave number from intensity scintillation measurements. Since a spectral break can be used to attenuate certain scale sizes in the structure, we use the two-component structure model as a framework for examining the relative contributions to the intensity field due to large- and small-scale ionospheric structures. These contributions are difficult to quantify directly due to the highly nonlinear response of the system. In this sense, investigation of the two-component model yields important insight into the general behavior of wave propagation in a random medium (irrespective of whether a well-defined spectral break at intermediate spatial scales is present). Finally, we generalize the commentary of *Uscinski et al*. [1981] by providing the conditions under which a general spectral break (representing an outer scale, inner scale, or intermediate scale) may be expected to influence the scintillation statistics.

2. The Statistical Theory of Scintillation

We begin by assuming that the effects of the disturbed ionosphere with statistically homogeneous refractive index fluctuations can be adequately represented by a thin phase-changing screen. We further assume that the fluctuations are formally two-dimensional, which is a suitable approximation for highly elongated field-aligned structure that results from the high mobility of electrons along magnetic field lines. The statistics of phase variations in the screen are characterized by the phase spectral density function $\Phi_{\delta\phi}(q)$. The phase structure function is defined as

$$D_{\delta\phi}(r) = \int_{-\infty}^{\infty} 2[1 - \cos(qr)]\,\Phi_{\delta\phi}(q)\,\frac{dq}{2\pi} \tag{1}$$

where r is the spatial separation and q is the corresponding spatial wave number. Under the paraxial approximation, the equation governing the fourth moment of intensity fluctuations assumes a parabolic form [*Ishimaru*, 1997; *Yeh and Liu*, 1982]. For the case of a normally incident plane wave, the solution for the intensity spectral density function (SDF) following traversal of the screen can be expressed as

$$\Phi_I(q) = \int_{-\infty}^{\infty} \exp\left[-g\left(r, q\rho_F^2\right)\right] \exp(-iqr)\,dr \tag{2}$$

where $\rho_F = \sqrt{z/k}$ is the Fresnel scale, z is the propagation distance from the screen, and k is the free-space wave number of the radio wave [*Gochelashvily and Shishov*, 1971; *Rino*, 1979b]. The structure interaction function that appears in (2) is given by the following combination of structure functions:

$$g(r_1, r_2) = D_{\delta\phi}(r_1) + D_{\delta\varphi}(r_2) - \frac{1}{2}D_{\delta\phi}(r_1 + r_2) - \frac{1}{2}D_{\delta\phi}(r_1 - r_2) \tag{3}$$

Using the half-angle angle identity, the structure interaction function can be written equivalently as [*Rino*, 1979b] equation (4):

$$g(r_1, r_2) = 8\int_{-\infty}^{\infty} \Phi_{\delta\phi}(q)\sin^2(r_1 q/2)\sin^2(r_2 q/2)\,\frac{dq}{2\pi} \tag{4}$$

The scintillation index, S_4, is obtained by integrating the intensity SDF over all wave numbers:

$$S_4^2 = \frac{1}{2\pi}\int_{-\infty}^{\infty} \Phi_I(q)\,dq - 1 \tag{5}$$

The unity term in (5) effectively removes the mean wave intensity, which is conserved in the calculation and set equal to unity. The intensity correlation function is the inverse Fourier (cosine) transform of the intensity spectrum:

$$R_I(r) = \int_{-\infty}^{\infty} \Phi_I(q)\cos(qr)\,\frac{dq}{2\pi} \tag{6}$$

which is commonly presented in normalized form as

$$\rho(r) = [R_I(r) - 1]/S_4^2 \tag{7}$$

The correlation length r_c is defined as the spatial separation for which the intensity correlation decreases to 50%, i.e., $\rho(r_c) = 1/2$.

2.1. The Two-Component Structure Model

Rino and Carrano [2013] proposed the following two-component model for the phase SDF corresponding to a 2-D irregularity model:

$$\Phi_{\delta\varphi}(q) = C_p' \begin{cases} |q|^{-p_1}, & q \le q_0 \\ q_0^{p_2-p_1}|q|^{-p_2}, & q > q_0. \end{cases} \tag{8}$$

The parameter C'_p is the strength of the phase SDF evaluated at 1 rad/m, and the prime is used to distinguish this from the phase spectral strength for the 3-D irregularity model described by *Rino* [1979a, 1979b]. Model (8) has a spectral break at the wave number q_0. The break wave number appears in the lower branch to force continuity of the spectrum at q_0. With this form $p_1 = p_2$ gives an unmodified power law, in which case we represent the phase spectral index with just p. The choice $p_1 = 0$ gives an outer scale, while the choice $p_2 \gg 3$ emulates an inner scale. It can be shown that the structure interaction function consistent with the two-component structure model is well defined provided that $p_1 < 5$ and $p_2 > 1$. Henceforth, we assume that the spectral indices satisfy these conditions (to avoid restating these conditions each time a new result is given). Moreover, we consider only cases of practical interest with $p_1 \le p_2$. Note that we colloquially refer to the spectral indices p_1 and p_2 as "slopes" when in fact they represent negative slopes in an inverse power law environment. Unless otherwise stated, we also generally assume that the Fresnel scale lies between the outer and inner scales, when the later are present. While we consider a strictly two-dimensional ionosphere in this paper, the appendix of the companion study [*Rino et al.*, 2016] demonstrates how this model may be related to the three-dimensional irregularity model described in *Rino* [1979a, 1979b]. In this case, the wave number q is reinterpreted as the square root of a quadratic form that depends on the magnetic field direction.

2.2. Self-Similar Form and Universal Scaling

The Fresnel scale arises naturally in diffraction calculations, even in a power law environment which lacks a dominant scale. We use the Fresnel scale to define a normalized spatial separation variable $\eta = r/\rho_F$ and a normalized wave number $\mu = q\rho_F$. This approach differs from that taken by previous authors who normalize by the outer scale [*Uscinski et al.*, 1981; *Bhattacharyya et al.*, 1992]. Since the presence of an outer scale may or may not have a significant influence on the intensity field, depending on the spectral shape and strength of scatter (we will show it has little influence when $p_1 \le p_2 < 3$), we argue the outer scale is not ideal for normalization.

In terms of the normalized variables, the phase SDF can be written as

$$P(\mu) = \begin{cases} U_1|\mu|^{-p_1}, & \mu \le \mu_0 \\ U_2|\mu|^{-p_2}, & \mu > \mu_0. \end{cases} \tag{9}$$

where the scattering strength parameters are given by

$$U_1 = C'_p \rho_F^{p_1-1}, \quad U_2 = C'_p q_0^{p_2-p_1} \rho_F^{p_2-1} \tag{10}$$

Note that (8) implies that the turbulent strength parameters are related as $U_2 = U_1 \mu_0^{p_2-p_1}$. Using (2), (4), and (9) the intensity spectrum can be expressed in dimensionless form as

$$I(\mu) = 2\int_0^\infty \exp\{-\gamma(\eta,\mu)\}\cos(\eta\mu)\,\mathrm{d}\eta \tag{11}$$

while the dimensionless structure interaction function becomes

$$\gamma(\eta,\mu) = 16\int_0^{\mu_0} U_1\chi^{-p_1}\sin^2(\chi\eta/2)\sin^2(\chi\mu/2)\frac{\mathrm{d}\chi}{2\pi} + 16\int_{\mu_0}^{\infty} U_2\chi^{-p_2}\sin^2(\chi\eta/2)\sin^2(\chi\mu/2)\frac{\mathrm{d}\chi}{2\pi} \tag{12}$$

In (12) the variable of integration $\chi = q\rho_F$ is a normalized wave number (like μ), and the integration is partitioned at the spectral break which occurs at the dimensionless wave number $\mu_0 = q_0\rho_F$.

The normalized phase and intensity spectra are related to their dimensioned counterparts as

$$\begin{aligned} P(\mu) &= \Phi_{\delta\phi}(\mu/\rho_F)/\rho_F \\ I(\mu) &= \Phi_I(\mu/\rho_F)/\rho_F \end{aligned} \tag{13}$$

Once the intensity spectrum (11) has been evaluated, the dimensional form of the spectrum can be recovered using (13). The scintillation index may be evaluated in terms of the normalized intensity spectrum as follows:

$$S_4^2 = \frac{1}{2\pi}\int_{-\infty}^{\infty} I(\mu)\mathrm{d}\mu - 1 \tag{14}$$

Similarly, the intensity correlation function may be expressed in terms of a normalized spatial separation distance $\xi = r/\rho_F$ as

$$\begin{aligned} R_I(\xi) &= \int_{-\infty}^{\infty} I(\mu)\cos(\mu\xi)\frac{\mathrm{d}\mu}{2\pi} \\ \rho(\xi) &= [R_I(r) - 1]/S_4^2 \end{aligned} \tag{15}$$

We define the universal scattering strength, U, as the normalized phase spectral power at the Fresnel scale,

$$U = \begin{cases} U_1, & \mu_0 \geq 1 \\ U_2, & \mu_0 < 1 \end{cases} \tag{16}$$

In other words, $U \equiv P(\mu = 1)$. For an unmodified power law we have $U = U_1 = U_2$, so that the two-component model reduces to the unmodified power law model discussed by *Rino and Owen* [1984]. When $U \ll 1$ the scatter is weak and when $U \gg 1$ the scatter is strong. The four parameters p_1, p_2, μ_0, and U specify all solutions for two-component spectra, in that different combinations of perturbation strength, propagation distance, and frequency produce the same results.

In a single power law environment the universal strength parameter $U = C'_p \rho_F^{p-1}$ admits the following interpretation. If a realization of a scale-free power law process is scaled by α^{p-1}, the scaled realization is statistically indistinguishable from the original realization. Since ρ_F controls the statistical structure, the diffraction theory must admit the same self-similar (fractal-like) scaling.

3. Summary of Asymptotic Results

Equations (11), (12), and (16) characterize the intensity SDF in normalized units as a function of a single universal strength parameter, U. From the intensity SDF, the scintillation index and the intensity correlation function follow. Thus, within practical constraints imposed by computation time, the complete parameter space can be explored. However, it is important to have checks and guidelines afforded by asymptotic limits. The complete catalog of results is extensive. Thus, we have chosen to present those details in a forthcoming sequel to this paper. Only the most important asymptotic results are summarized here. The purpose of presenting this summary here is twofold. First, the asymptotic formulas are used to validate the numerical results. Second, the asymptotic results organize the behavior of the intensity SDF in terms of different classes of irregularity spectra and guide the interpretation of the numerical experiments conducted in this paper.

3.1. Weak Scatter

When the scatter is weak ($U \ll 1$), the exponential in (11) may be expanded in a Maclaurin series to first order and (12) may be used to obtain the well-known result [*Yeh and Liu*, 1982]:

$$I(\mu) = 2\pi\delta(\mu) + \left[4\sin^2\left(\mu^2/2\right)\right]P(\mu) \tag{17}$$

The interpretation is that in weak scatter the intensity SDF is a Fresnel-filtered version of the structure (phase) SDF, where the so-called Fresnel filter function appears in brackets. The filter function acts to suppress the contribution from large-scale structure. The approximation (17) is also generally applicable (for any strength of scatter) at sufficiently small and large wave numbers, except that the Fresnel oscillations are suppressed in strong scatter [*Gochelashvily and Shishov*, 1971]. The behavior at low wave numbers follows by expanding the Fresnel filter function in a Maclaurin series to the lowest order:

$$I(\mu) \sim |\mu|^4 P(\mu) \tag{18}$$

The behavior at large wave numbers follows by noting that the Fresnel filter function oscillates about a value 2

$$I(\mu) \sim 2P(\mu) \tag{19}$$

For the two-component power law model, (18) and (19) indicate a return to power law behavior at asymptotically small and large wave numbers. The range of intermediate wave numbers over which deviations from power law behavior may occur and neither approximation (18) nor (19) is applicable increases with increasing strength of scatter U.

In the weak scatter approximation, the behavior of the scintillation index S_4 may be inferred by substituting (17) into (11). The complete result will be given in a forthcoming sequel to this paper, but the dependence on scattering strength is such that $S_4^2 \propto U$. Under the same weak scatter approximation, the normalized intensity correlation function $\rho(\xi)$ is independent of the strength of scatter U. This can be seen by substituting (17) into (5) and (6) to find that $R(\xi) \propto U$ and $S_4^2 \propto U$, respectively, such that the scattering strength cancels out in the defining relation (7). The normalized intensity correlation length ξ_c is therefore also independent of scattering strength and in fact is an order one quantity that depends only on p_1, p_2, and μ_0. As such, the dimensioned intensity correlation length r_c varies like the Fresnel scale in weak scatter. In particular, r_c increases with propagation distance past the phase screen.

3.2. Strong Scatter

Under moderate scatter conditions ($U \sim 1$) the increase in the scintillation index with increasing strength of scatter is not as easily summarized. As the scattering strength increases the scintillation index will ultimately saturate at a limiting value that may exceed unity. The transition to saturation can proceed either without exceeding unity or by reaching a strong focusing maximum. Once the scintillation index begins to saturate, the normalized correlation length begins to decrease with increasing strength of strength. Here we summarize the behavior of the scintillation index and correlation length for the case of asymptotically large U. The limiting behavior can be shown to depend critically on the spectral index p_1 of the two-component model at low wave numbers. All of the asymptotic results presented in this section are new.

When $p_1 < 3$ (which includes the case when an outer scale is present), the limiting value of the scintillation index is unity. The approach to this limit may be monotonic, or a local maximum may be achieved with $S_4 > 1$ due to strong focusing. In the latter case, the scintillation index will recede from its maximum value with increasing strength of scatter, ultimately converging to unity from above. This behavior has been discussed extensively by previous authors [e.g., *Salpeter*, 1967; *Singleton*, 1970; *Gochelashvily and Shishov*, 1971].

When $3 < p_1 < 5$, the limiting value is

$$S_4 \to \sqrt{\frac{p_1 - 1}{5 - p_1}} \tag{20}$$

which exceeds unity. This so-called quasi-saturation state, whereby S_4 approaches a value exceeding unity in the strong scatter limit, occurs only when $p_1 > 3$. In this case the value of p_2 is immaterial in the sense that the large-scale phase structure ($\mu < \mu_0$) dominates the development via strong focusing. *Rino* [1979b] and *Rino and Owen* [1984] derived a result for the case of an unmodified power law spectrum which is less than the limiting value (20) because the contribution from low frequencies was neglected in their analysis. In fact, the low-frequency contribution becomes increasingly significant as p_1 exceeds 3 due to strong focusing effects. It should be noted, however, that the irregularities must be homogenous for the statistical theory to be valid (i.e., the structure must admit Fourier decomposition). If the irregularities are inhomogeneous at the largest scales, then departures from the strong scatter theory may be expected if these large-scale structures play a significant role in the scattering.

As mentioned earlier, the normalized intensity correlation length ξ_c is independent of scattering strength in weak scatter ($U \ll 1$). The normalized correlation length begins to develop a dependence on scattering strength in the transition region ($U \sim 1$). In the strong scatter limit ($U \to \infty$) this dependence takes the form of an inverse power law, $\xi_c \propto U^{-n_c}$, where the exponent n_c depends on p_1 and p_2 from the two-component model. An exception is the special case $p_1 = p_2 = 3$ which will be discussed later. To simplify the notation below, let $\beta_1 = 1$ if $\mu_0 \geq 1$ and $\beta_1 = \mu_0^{p_1 - p_2}$ if $\mu_0 < 1$ so that $U_1 = \beta_1 U$. Similarly, let $\beta_2 = \mu_0^{p_2 - p_1}$ if $\mu_0 \geq 1$ and $\beta_2 = 1$ if $\mu_0 < 1$ so that $U_2 = \beta_2 U$.

3.2.1. Shallow Spectra

When $p_1 \leq p_2 < 3$, the limiting correlation length takes the following form:

$$\xi_c \to \left[\frac{\log(2)}{U\beta_2} \left(\frac{\sqrt{\pi}(p_2 - 1)\Gamma\left[\frac{p_2}{2}\right]}{2^{2-p_2}\Gamma\left[\frac{3-p_2}{2}\right]} \right) \right]^{1/(p_2 - 1)} \tag{21}$$

Thus, $n_c = 1/(p_2 - 1)$ which tends to 1/2 as p_2 approaches 3. If $p_1 = p_2$, we recover the result for an unmodified power spectrum. It is clear from (21) that the limiting correlation length is dictated by the high-frequency portion of the phase spectrum ($\mu > \mu_0$) when it is shallow, as might be expected. In fact, if $\mu_0 < 1$, the limiting correlation length is the same as for an unmodified power law with $p = p_2$.

3.2.2. Steep Spectra

If $p_2 \ge p_1 > 3$, the limiting normalized correlation length can be shown to satisfy the following integral equation:

$$\int_{-\infty}^{\infty} |\mu|^{-(p_1-3)/2} \exp\left[-\frac{|\mu|^{5-p_1}}{4AU}\right] \exp(-i\mu\xi_c)\, \mathrm{d}\mu = 2\sqrt{AU\pi} \tag{22}$$

where

$$A = \beta_1 \frac{2^{2-p_1}(p_1-2)\Gamma\left[\frac{5-p_1}{2}\right]}{\sqrt{\pi}(p_1-3)\Gamma\left[\frac{p_1}{2}\right]} \tag{23}$$

In general, (22) must be solved numerically to determine the limiting correlation length. Having done so, we present the following empirical fit which provides a useful approximation when $3 < p_1 \le 4$:

$$\xi_c \rightarrow \frac{0.32 + 1.4(p_1-3) + \exp[-6.2 + 7.2(p_1-3)]}{(\beta_1 U)^{1/(5-p_1)}} \tag{24}$$

When $p_1 > 4$, a better approximation may be obtained by replacing the leftmost exponential in (22) with unity. Performing the integration and solving for ξ_c give

$$\xi_c \rightarrow \left[\frac{1}{\beta_1 U}\Gamma\left[\frac{5-p_1}{2}\right]\Gamma\left[\frac{p_1}{2}\right]\frac{2^{p_1-1}(p_1-3)[1+\sin(p_1\pi/2)]}{(p_1-2)}\right]^{\frac{1}{5-p_1}} \tag{25}$$

In summary, when $p_1 > 3$, the correlation length is an inverse power law function of the scattering strength with exponent $n_c = 1/(5-p_1)$, which tends to 1/2 as p_1 approaches 3. The limiting correlation length on scattering strength is dictated by the low-frequency portion of the phase spectrum ($\mu < \mu_0$) when it is steep.

3.2.3. Mixed-Slope Spectra

When $p_1 < 3$, $p_2 > 3$, the limiting correlation length is

$$\xi_c \rightarrow \left[\frac{\log(2)}{U\beta_1\mu_0^{3-p_1}}\frac{\pi(p_2-3)(3-p_1)}{(p_2-p_1)}\right]^{1/2} \tag{26}$$

In this case the limiting correlation length is an inverse power law function of the scattering strength U with exponent $n_c = 1/2$, irrespective of the values of p_1 and p_2. This dependence is due to the leading term in the Maclaurin series expansion of the structure function, which depends quadratically on the spatial separation under these conditions. Interestingly, the rate at which ξ_c decreases with increasing scattering strength is slower for mixed-slope spectra than that for an unmodified power law with *any* slope (except for the special case $p_1 = p_2 = 3$, which is discussed next). This is true whether the break acts as an outer scale, and intermediate spectral break, or an inner scale. Mixed-slope spectra are thus more inherently "balanced" than shallow or steep spectra, in the sense that they lack an overabundance of large-scale structure (which causes strong focusing) and small-scale structure (which scatters waves more effectively and tends to mitigate these focusing effects).

For an unmodified power law with $p_1 = p_2 = 3$ the limiting correlation length departs from a strictly inverse power law dependence on scattering strength and instead behaves as

$$\xi_c \rightarrow \left[\frac{2}{U\log(U)}\right]^{1/2} \tag{27}$$

This rate of decrease with increasing scattering strength is the slowest for any one- or two-component inverse power law. In a sense, this case represents the point of balance where neither the large- nor small-scale structure dominates the development in the strong scatter regime. For steeper spectra the intensity field becomes dominated by the large-scale structure, while for shallower spectra it becomes dominated by the small-scale structure provided the scatter is sufficiently strong. This interpretation also holds for general two-component spectra, but in this case the development depends on the two slopes and the location of the spectral break relative to the Fresnel scale.

4. Numerical Results and Discussion

We begin this section by briefly describing the numerical techniques used to compute the intensity SDF. This is followed by a discussion of our numerical experiments. Since the integral defining the intensity SDF (11) is oscillatory over the unbounded domain $(0, \infty)$, specialized quadrature methods are recommended for its numerical evaluation. Having experimented with many techniques, we found the most efficient to be the double exponential quadrature scheme for Fourier-type integrals developed by *Ooura and Mori* [1991]. This scheme employs a specialized transformation that ensures the transformed integrand decreases rapidly (doubly exponentially) while at the same time clustering quadrature nodes near the zeroes of the cosine function. As a result, a truncated quadrature sum will achieve rapid convergence with increasing number of terms for Fourier-type integrals with slowly (algebraically) decaying integrands. This algorithm employs an adaptive grid for the quadrature, using as many nodes as required to achieve the desired accuracy. This has an advantage over numerical techniques that solve the fourth moment equation on a fixed grid (e.g., the method of finite differences [*Gozani*, 1985] or the split-step method [*Bhattacharyya and Yeh*, 1988]). The reason is that the range of η values over which the integrand must be evaluated to achieve a prespecified accuracy depends critically on the scattering strength. Fixed grid techniques can produce incorrect or misleading results when using an unmodified power law structure model; the fixed grid implicitly imposes inner and outer scales on the structure which can significantly alter the development of the scintillation.

While it is possible to evaluate the structure interaction function (12) via numerical quadrature, this becomes increasingly difficult when $\eta/\mu \ll 1$ or $\eta/\mu \gg 1$ because the integrand contains oscillations with two highly separated frequencies. As it happens, this condition is met for larger number of quadrature nodes as the strength of scatter increases. We avoided this problem by calculating the structure interaction function using an analytic formula derived in a forthcoming sequel to this paper. When $\eta/\mu \ll 1$ or $\eta/\mu \gg 1$, however, direct evaluation of this formula results in catastrophic loss of precision due to the subtraction of nearly equal terms. We avoided this by expanding the structure interaction function in a Maclaurin series (summing additional terms until convergence is reached). Because of the potentially large dynamic range of the intensity SDF when the scatter is strong, all calculations were performed using the Mpmath Python library for arbitrary-precision floating-point arithmetic [*Johansson et al.*, 2013]. It was determined by numerical experimentation that retaining 64 digits for these calculations produced highly accurate results. It was not always possible, for example, to demonstrate the high-frequency return to power law behavior in very strong scatter conditions using IEEE double precision with 16 digits. The Python software used to produce all the numerical results in this paper is available from the authors upon request. Next, we describe results of our numerical experiments.

4.1. Morphology of the Intensity Spectrum

In this section we investigate the shape of the intensity spectrum as a function of frequency and scattering strength. We compare the cases of an unmodified power law, a modified power law with an outer scale, and a modified power law with an inner scale. At this point it is useful to introduce the notion of a "dominant" spectral index. We define the dominant spectral index p for a two-component spectrum to be the (negative) slope of the phase spectrum at the Fresnel frequency ($\mu = 1$); in other words $p = p_1$ if $\mu_0 \geq 1$ and $p = p_2$ if $\mu_0 < 1$. This notion is most useful when the spectral break is well separated from the Fresnel frequency (i.e., $\mu_0 \ll 1$ or $\mu_0 \gg 1$). In the discussion that follows we will impose outer and inner scales on an initially unmodified power law of index p. Even though the introduction of an outer or inner scale formally creates a two-component spectrum, at times we may continue to refer to the index p only (rather than explicitly mentioning both p_1 and p_2). It should be understood in these cases that the dominant spectral index is intended. We begin by considering the case of an unmodified power law with $p_1 = p_2 = p$.

Figure 1 shows the behavior of the intensity spectrum in the receiver plane following propagation through the phase screen. The irregularities are characterized by an unmodified inverse power law with half-integer values of the phase spectral index ranging from $p = 1.5$ to $p = 4.5$. Results corresponding to four values of the universal scattering strength are shown in each panel, ranging from $U = 1$ to $U = 1000$. Note that the axes for the cases $p = 1.5$ and $p \geq 4$ are significantly different from the others; this was necessary to capture the dynamic range of interest (in particular, the return to power law behavior at asymptotically small and large wave numbers). For all values of scattering strength the intensity spectrum returns asymptotically to power law behavior at low and high wave numbers with $I(\mu) \sim U|\mu|^{4-p}$ and $I(\mu) \sim 2\,U|\mu|^{-p}$, respectively. These asymptotes are shown as gray dashed lines in Figure 1. Between these power law regions lies a more gently sloped "plateau" region that includes the Fresnel wave number $\mu = 1$. Note that the large-scale intensity structure is partially suppressed by the action of Fresnel filtering. However, the efficacy of this large-scale suppression is decreased as the phase spectral index increases (since the filter acts a power law multiplier in the frequency domain with a fixed exponent, i.e., $|\mu|^4$).

When $U \ll 1$, the intensity spectrum (not shown) exhibits Fresnel oscillations as suggested by the weak scatter result (17). As U increases these Fresnel oscillations are gradually suppressed, and for some critical values of

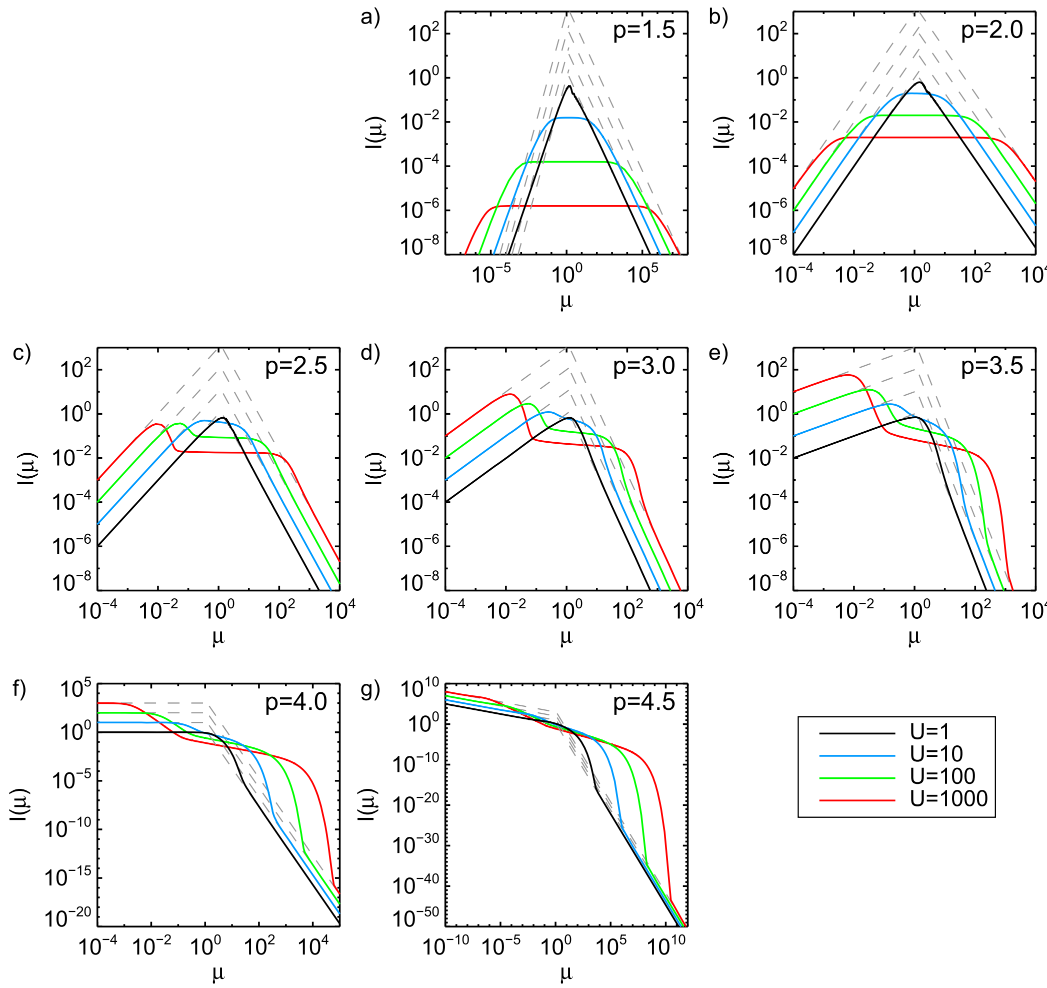

Figure 1. Spectra of intensity variations in the receiver plane following propagation through irregularities characterized by an unmodified power law. The different panels show results for values of the phase spectral index ranging from $p = 1.5$ to $p = 4.5$. The different colored curves correspond to the scattering strength values $U = 1$, 10, 100, and 1000.

scattering strength $U \approx 1$ the spectrum resembles a smooth concatenation at the Fresnel wave number $\mu = 1$ of the small and high wave number inverse power law asymptotes. The critical value of U at which this occurs decreases for increasing p. These strong scatter effects are first manifested at lower values of U for more steeply sloped spectra. As U increases further the intensity spectrum widens, extending to both smaller and larger wave numbers, while the power in the plateau region surrounding the Fresnel wave number decreases accordingly to maintain saturation (or quasi-saturation) conditions (specifically, S_4 approaches unity when $p < 3$ and S_4 approaches the result (20) when $3 < p < 5$). Thus, there is necessarily a significant departure from power law behavior at intermediate wave numbers when $U \gg 1$. *Rumsey* [1975] analyzed the 3-D isotropic case rather than the 2-D case that we consider, but he also noted that for any given scattering strength the intensity spectrum widens without bound as p approaches either end of its permissible range (in our case the values 1 and 5). From the form of (11) it is evident that as the strength of scatter increases the contribution to the intensity spectrum at large μ originates predominantly from small values of η and vice versa. This effect is stronger for more steeply sloped spectra. This fact, together with (12), implies that as the intensity spectrum widens so does the range of spatial scales in the ionospheric structure that contributes appreciably to the integral (11). For a given value of U, the least spectral widening (at both low and high wave numbers) occurs for the case $p = 3$, which (as we shall see) also corresponds to the case of the longest intensity correlation length for any $1 < p < 5$.

For the cases with $p > 2$ the approach to the low wave number asymptote takes the form of a low-frequency enhancement, while the approach to the high wave number asymptote may involve significant overshoot referred to as high-frequency spectral broadening [*Booker and MajidiAhi*, 1981; *Forte*, 2008, 2012; *Carrano*

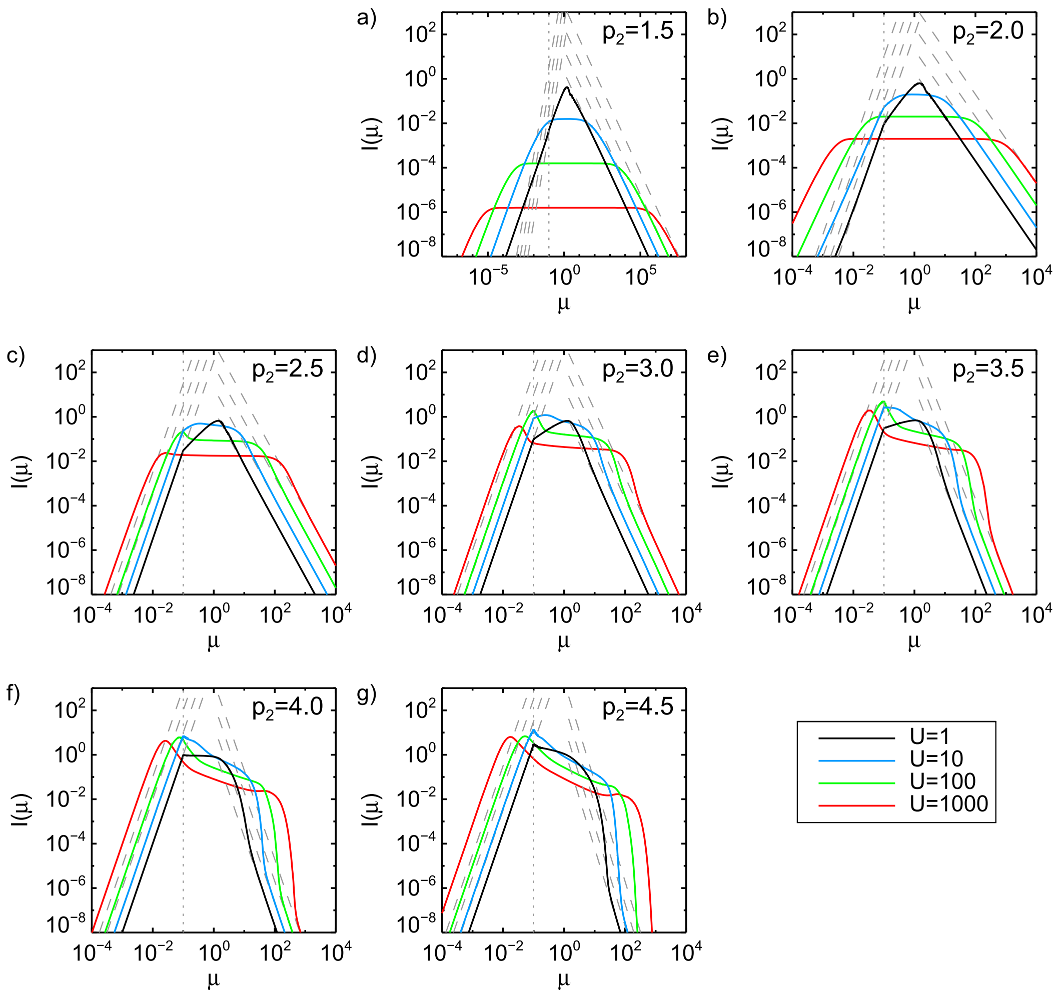

Figure 2. Spectra of intensity variations in the receiver plane following propagation through irregularities characterized by a modified power law with an outer scale ($p_1 = 0$) imposed at the wave number $\mu_0 = 0.1$. The different panels show results for values of the high-frequency phase spectral index ranging from $p_2 = 1.5$ to $p_2 = 4.5$. The different colored curves correspond to the scattering strength values $U = 1$, 10, 100, and 1000.

et al., 2012]. Progressively steeper spectra with $p > 2$ exhibit more high-frequency broadening. Both effects are associated with strong focusing conditions which produce S_4 values that exceed unity. In all of our simulations, a clear return to power law behavior is observed at high frequencies. This return to power law behavior at high frequencies is quite gradual for shallow spectra ($p < 3$) and abrupt for steep spectra ($p > 3$). While this return to power law is quite prominent for steep spectra, it occurs where the intensity SDF is small and therefore may go unnoticed in many experiments. We also observed a clear return to power law behavior at low frequencies when $p \geq 2$. When $p < 2$, there was a tendency to approach the theoretically predicted asymptotic slope (if not the scale factor). This anomaly appears to be a consequence of the fact that as the phase spectral index approaches the singular value $p = 1$ from above, an increasingly broad range of structure scales contributes to the intensity spectrum at small wave numbers. In this case, higher-order terms than those retained in the derivation of (18) are required to establish the correct asymptotic result. We note that the intensity spectra presented by *Booker and MajidiAhi* [1981] do not exhibit a clear return to power law behavior at large wave numbers because the SDF they used to describe the structure included an inner scale with exponential falloff.

Figure 2 shows the behavior of the intensity spectrum in the receiver plane following propagation through the phase screen when the irregularities are modeled by a modified inverse power law with an outer scale (much larger than the Fresnel scale). The outer scale is imposed with $p_1 = 0$ and at the break wave number $\mu_0 = 0.1$. The various panels in the figure correspond to half-integer values of the high-frequency slope p_2 ranging from $p_2 = 1.5$ to $p_2 = 4.5$ (i.e., the dominant spectral index $p = p_2$ is varied). The vertical dotted line indicates the break wave number. When a spectral break is present, the intensity spectrum for asymptotically small and large μ behaves like $I(\mu)\tilde{\ }\mu^{4-p_1}$ and $I(\mu)\tilde{\ }2\mu^{-p_2}$, respectively. These asymptotes are shown as gray dashed lines in Figure 2.

Note that when the scatter is weak, the spectral break is easily discernible as a discontinuity in the slope of the intensity spectrum. This discontinuity is present in weak scatter because each harmonic in the intensity variations is proportional to the corresponding harmonic in the phase screen according to (17). When the scatter is strong, the presence of a spectral break is no longer directly apparent in the intensity spectrum. This occurs because when the scatter is strong, the contribution to each harmonic in the intensity spectrum comes from many harmonics in the screen through the nonlinearity implied by (11) [see also *Hewish*, 1989]. Similarly, the contribution from harmonics in the screen near the spectral break is distributed to many harmonics in the intensity field, effectively smoothing out the discontinuity. We also note that for large $U \gg 1$ the return to power law behavior at low wave numbers is consistent with the slope, but not the scale factor, of the theoretical result (18).

A comparison of Figures 1 and 2 reveals the effect of an imposed outer scale (much larger than the Fresnel scale) on the development of the intensity fluctuations in the receiver plane. The shallow spectra cases with $p < 3$ are affected by the presence of the outer scale only in the vicinity of the break wave number $\mu_0 = 0.1$ and smaller wave numbers (compare Figures 2a–2c with their counterparts in Figure 1). The effects of the outer scale are relatively subtle for these shallow spectra; the low-frequency enhancement is partially suppressed, and the return to power law behavior at low wave numbers is achieved with a steeper (positive) slope. Conversely, the steeply sloped spectra cases with $p > 3$ exhibit dramatically less spectral dynamic range at both low and high wave numbers when the outer scale is present (compare Figures 2e–2g with their counterparts in Figure 1). The reason for this differing response to the presence of an outer scale for shallow and steep spectra has to do with the presence and efficacy of large-scale focusing. When the scatter is strong, large-scale features in the ionospheric structure tend to focus the radio waves, resulting in the generation of intensity variations with scales both large and small [*Mercier*, 1962; *Booker and MajidiAhi*, 1981; *Hewish*, 1989]. The imposition of an outer scale has a greater effect in the case of a steeply sloped spectrum primarily because it results in the erosion of comparatively more large-scale structure than in the case of a shallow spectrum.

Figure 3 shows the behavior of the intensity spectrum in the receiver plane following propagation through the phase screen when the irregularities are modeled by a modified inverse power law with an inner scale (much smaller than the Fresnel scale). The inner scale is emulated with $p_2 = 4.5$ imposed at the break wave number $\mu_0 = 10$. The various panels correspond to half-integer values of the low-frequency index p_1 ranging from $p_1 = 1.5$ to $p_1 = 4.5$ (i.e., the dominant spectral index $p = p_1$ is varied). The vertical dotted line indicates the break wave number, and the gray dashed lines delineate the high- and low-frequency asymptotes. The case $p_1 = 4.5$ actually has no spectral break since $p_1 = p_2$. As in the case of an outer scale, the presence of the current spectral break (representing an inner scale) is only directly evident as a discontinuity in the slope of the intensity spectrum when the scatter is weak. When the scatter is strong, nonlinear interactions result in a smoothed intensity spectrum. In the strong scatter case the introduction of an inner scale has a dramatic effect on the shallow sloped cases $p < 3$ (compare Figures 3a–3c with their counterparts in Figure 1). The inner scale limits the dynamic range of $I(\mu)$ for the shallow spectrum cases considerably, and the small-scale enhancement is larger than that for the unmodified power law case. The inner scale has almost no effect on the steeply sloped cases $p > 3$ (compare Figures 3e–3g with their counterparts in Figure 1). The reason for this differing response for shallow and steeply sloped spectra has once again to do with the presence and efficacy of large-scale focusing. Focusing by the large-scale features transpires under strong scatter conditions regardless of the spectral slope. However, shallower spectra imply the increased presence of small-scale structure which tends to scatter the radio waves more effectively (in a wider range of directions), thereby reducing the net efficacy of large-scale focusing [*Alimov and Rakhlin*, 1996; *Vats et al.*, 1981; *Bhattacharyya et al.*, 2003].

4.2. Irregularity Parameter Estimation

One of the principal uses of the two-component model is to aid with the interpretation of scintillation data obtained from an experiment. The goal is to relate measurable characteristics of the measured signal fluctuations to the statistical characteristics of the random medium responsible for producing the scintillations. One approach for accomplishing this is to use nonlinear least squares techniques to fit the intensity SDF of the measurements with that obtained from (11); if the effective scan velocity [*Rino*, 1979a] is known, this approach provides the four phase screen parameters p_1, p_2, μ_0, and U. We refer to this as irregularity parameter estimation (IPE), since the parameters defining a statistical description of the irregularities are

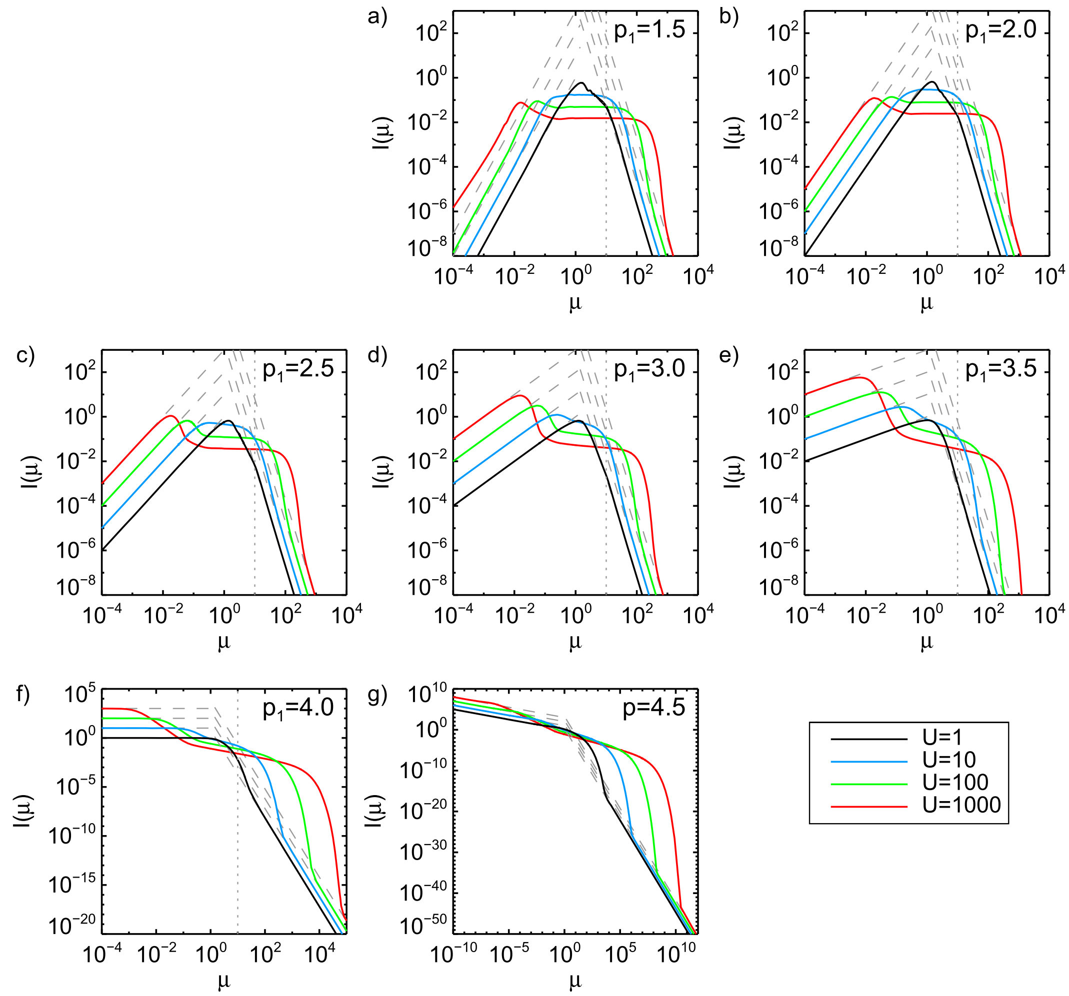

Figure 3. Spectra of intensity variations in the receiver plane following propagation through irregularities characterized by a modified power law with an effective inner scale ($p_1 = 4.5$) imposed at the wave number $\mu_0 = 10$. The different panels show results for values of the low-frequency phase spectral index ranging from $p_1 = 1.5$ to $p_1 = 4.5$. The different colored curves correspond to the scattering strength values $U = 1$, 10, 100, and 1000.

retrieved from the scintillation observations. A similar approach was used by *Carrano et al.* [2012] in conjunction with a different scintillation model. Figure 4 shows an example whereby the SDFs of intensity scintillation measurements at VHF (244 MHz) and L band (1535 MHz) have been fit with those obtained from (11) to infer the model parameters p_1, p_2, μ_0, and U. These measurements were acquired by Air Force Research Laboratory on 22 March 2000 by monitoring VHF and L band geostationary satellite signals at Ascension Island (7.96°S, 14.41°W). The VHF and L band links were nearly colinear, with ionospheric penetration points separated in the magnetic east-west direction by only 38 km, enabling a multifrequency analysis of scintillations along (nearly) the same propagation geometry. The VHF data were acquired using antennas spaced in the magnetic east-west direction, which enabled direct measurement of the zonal irregularity drift and calculation of the effective scan velocity. This velocity was used to map the measured scintillation time series to spatial series, and the L band data were subsequently advanced by 38 km to approximately align it with the VHF data. The SDFs were computed by applying Welch's method to a 4 min period of data using a sliding 2 min window with 50% overlap [*Welch*, 1967]. The least squares fits were performed over the wave number range shown in Figure 4 with gray shading. We exclude from the fix the lowest frequencies which may be distorted by large-scale departures from stationarity and also the highest frequencies which may be contaminated by receiver noise. The result of the least squares spectral fitting of both the VHF and L band intensity SDFs using the same irregularity model yielded estimates for the low- and high-wave number phase spectral indices $p_1 = 2.2$ and $p_2 = 3.8$ with a spectral break at $L_0 = 957$ m (which translates to the break wave numbers $\mu_0 = 1.7$ at VHF and $\mu_0 = 0.7$ at L band).

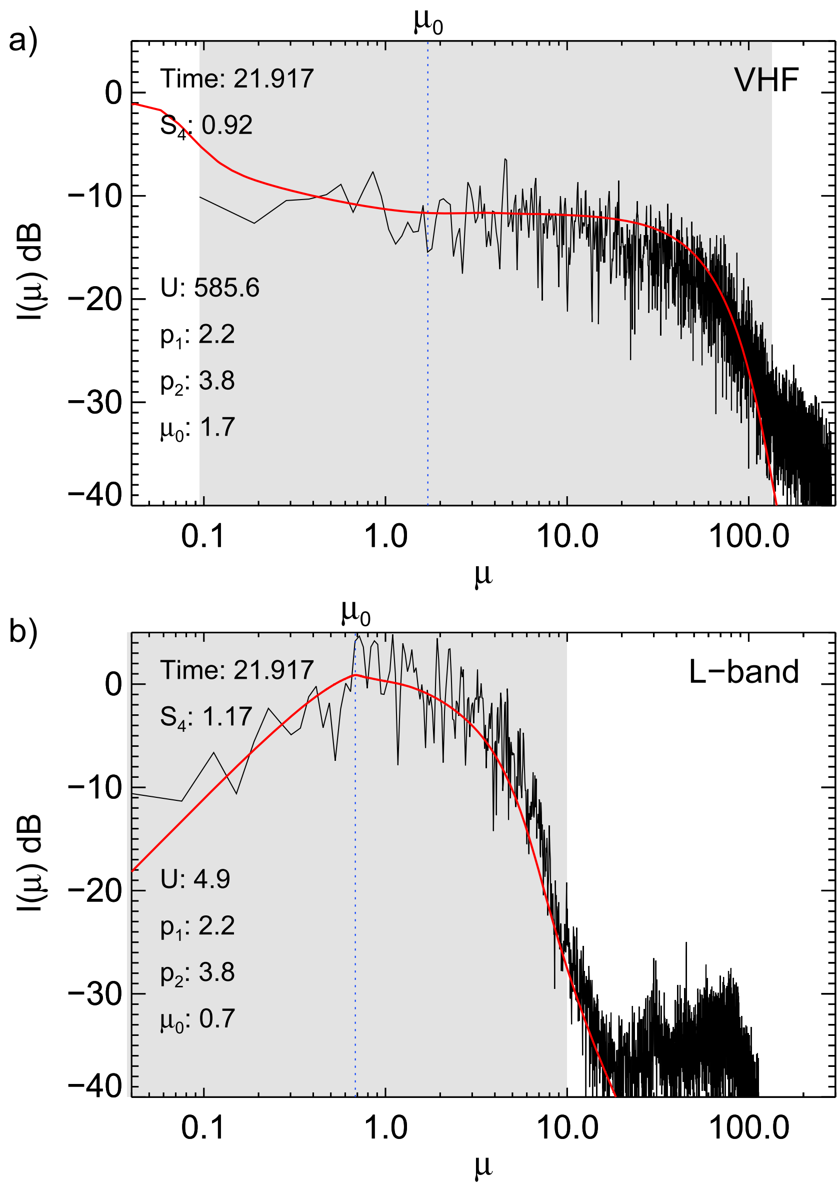

Figure 4. Spectral density functions for intensity scintillations observed at (a) VHF and (b) L band. The SDFs for the measurements are shown in black, while the fitted model SDFs are shown in red. The gray shaded area indicates the wave number range over which the fits were performed. The wave number of the inferred spectral break is shown with a blue dotted line.

The two-component irregularity model is necessary to reconcile these scintillation observations at VHF and L band. We note that both VHF and L band scintillations are in the strong scatter regime ($U > 1$) with $U = 585.6$ at VHF and $U = 4.9$ at L band. Also note that the S_4 index is slightly larger at L band ($S_4 = 1.17$) than it is at VHF ($S_4 = 0.92$), which is a consequence of modest strong focusing effects on the higher-frequency signal. It should be noted that the S_4 value (0.92) computed from the VHF measurements is less than unity because the 4 min period used to compute this statistic is not sufficiently long to capture the largest-scale signal fluctuations. Integrating the fitted model SDF (red curve in Figure 4a) over all wave numbers gives $S_4 = 1.01$, indicating that saturation conditions have indeed been attained. Previous authors have used the *Booker and MajidiAhi* [1981] strong scatter calculations to interpret scintillations in either qualitative [*Forte*, 2008, 2012] or quantitative ways [*Vats et al.*, 1981]. In none of these studies were the irregularity parameters estimated by least squares fitting of the data, possibly because the *Booker and MajidiAhi* [1981] results are available only for integer and half-integer values of the phase spectral index. Our model allows for arbitrary fractional values of the spectral indices, which makes it better suited for least squares fitting.

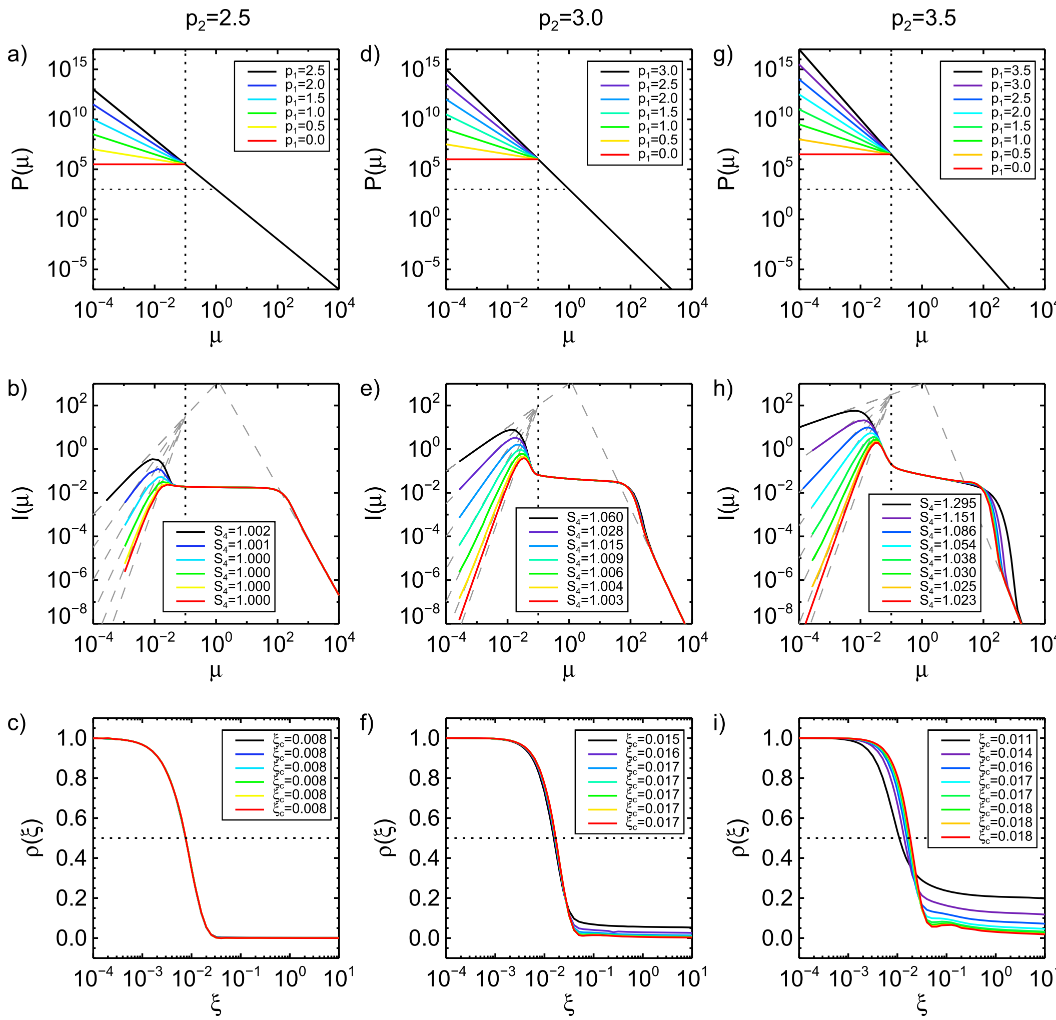

Figure 5. Effect of an outer spectral break at wave number $\mu_0 = 0.1$ under strong scatter conditions with $U = 1000$. The individual panels show the (a, d, and g) phase spectra, (b, e, and h) intensity spectra, and (c, f, and i) intensity correlation functions for different values of the low-frequency spectral index p_1 when the high-frequency spectral index is $p_2 = 2.5$ (Figures 5a–5c), $p_2 = 3.0$ (Figures 5d–5f), and $p_2 = 3.5$ (Figures 5g–5i).

One is often tempted to estimate the spectral indices more simply by fitting the measured intensity SDF with a line in log-log space. The question that arises when doing so is, in what frequency range should this linear fit be performed? When the scatter is strong, this question may have no easy answer. Figures 1–3 demonstrate that the local slope of the intensity SDF is equal to one of the (negative) spectral indices of the model (p_1 or p_2) only at extremal wave numbers (i.e., following the return to power law behavior at asymptotically low and high wave numbers). Since the intensity SDF has less power at extremal wave numbers, it is often the case that the return to power law behavior occurs below the noise floor of the measurement system. When this occurs, departures from power law behavior at measurable scales preclude obtaining reliable estimates of the spectral indices via the simple linear fitting approach. For example, the measured SDFs shown in Figure 4 exhibit no power law wave number range over which the spectral indices may be reliably measured by fitting a line in log-log space. The resolution to this problem is to fit the SDF of measurable intensity variations with the model intensity SDF obtained from (11) over as wide a wave number range as possible (while avoiding nonstationarity effects and receiver noise).

4.3. Contributions From Large- and Small-Scale Irregularity Structures

In this section we consider the ramifications of a spectral break in more detail. Our purpose is to investigate the relative contributions to the scintillation from large- and small-scale ionospheric structures. This is difficult to quantify except through simulation when the scatter is strong, due to the highly nonlinear response of the system.

Figure 5 shows the effect of an outer spectral break ($\mu_0 = 0.1$) under strong scatter conditions ($U = 1000$). Three high-frequency spectral indices are considered: one shallow ($p_2 = 2.5$), one intermediate ($p_2 = 3.0$), and one steep ($p_2 = 3.5$). Several values of the low-frequency index p_1 are considered, ranging from the value of p_2 (which yields an unmodified power law) down to zero (which imposes an outer scale). The effect of the outer spectral break is to increasingly erode large-scale irregularity structure as p_1 is decreased. Figures 5a, 5d, and 5g show the phase spectrum, Figures 5b, 5e, and 5h the intensity spectrum, and Figures 5c, 5f, and 5i the intensity correlation function. For the spectral plots, the dashed lines show theoretical low- and high-frequency asymptotes, the vertical dotted line indicates the break scale, and the horizontal dotted line indicates the value of the phase spectral strength evaluated at the Fresnel scale, which is equal to the universal strength of scatter U. The horizontal dotted line in the intensity correlation plots indicates 50% decorrelation, the abscissa at which location is equal to the intensity correlation length ξ_c. Values of S_4 and normalized correlation length ξ_c for the different curves (corresponding to different values of p_1) are labeled on the panels for convenience.

As is evident from Figures 5a–5i, eroding large-scale structure suppresses development of the low-frequency enhancement for the shallow spectrum case ($p_2 = 2.5$). For the steeply sloped case ($p_2 = 3.5$), eroding large-scale structure suppresses both low-frequency variations and also the prominent spectral broadening at high frequencies. From this we infer that strong focusing by large-scale irregularity structure is responsible for both the low-frequency enhancement and high-frequency spectral broadening. For the shallow spectrum case, the presence or absence of a low-frequency enhancement does not alter S_4 (Figure 5b) or the intensity correlation length (Figure 5c). On the other hand, for the steeply sloped spectrum case, suppressing the low-frequency variations and high-frequency spectral broadening drives S_4 from its quasi-saturation value (20) down to unity (Figure 5 b), alters the shape of the correlation function (Figure 5i), and significantly increases the correlation length. For the intermediate slope case ($p_2 = 3.0$), other than suppression of the low-frequency enhancement, the erosion of large-scale structure has little effect. The S_4 value remains close to unity (Figure 5e), and the correlation function exhibits a change only at large spatial separations (Figure 5f), leaving the correlation length unchanged.

Figure 6 shows the effect of an inner spectral break ($\mu_0 = 10$) under strong scatter conditions ($U = 1000$). Three low-frequency spectral slopes are considered: one shallow ($p_1 = 2.5$), one intermediate ($p_1 = 3.0$), and one steep ($p_1 = 3.5$). Several values of the high-frequency index p_2 are considered, ranging from the value of p_1 (which yields an unmodified power law) to 4.5 (which emulates an inner scale). The panel layout and labeling are otherwise identical to Figure 5. In this case, the effect of the inner break is to increasingly erode small-scale irregularity structure as p_2 is increased. For the shallow spectra case ($p_1 = 2.5$) this significantly reduces the width of the intensity spectrum and increases the correlation length compared to that for an unmodified power law irregularity spectrum. Since the small-scale content in the intensity SDF is suppressed by eroding the small-scale irregularity structure, we can conclude that the latter is responsible for generating the small-scale intensity variations. As explained by *Booker and MajidiAhi* [1981], these small-scale intensity variations are generated by small-scale irregularities via diffractive processes. Interestingly, the erosion of small-scale structure promotes focusing by the larger-scale structure that remains. Note that this focusing actually increases the fluctuation power in the intensity SDF at all scales between the low-frequency return to power law and the spectral break. A number of researchers [*Bhattacharyya et al.*, 1992, 2003; *Engavale and Bhattacharyya*, 2005] have observed that the presence of small-scale structure associated with fully developed plasma turbulence at low latitudes in the early postsunset hours tends to suppress strong focusing and inhibit S_4 values exceeding unity. By late evening diffusive processes have eroded the small-scale structure, which encourages strong focusing and can result in S_4 values well above unity. Figures 6g, 6h, and 6i show that for steep spectra ($p_1 = 3.5$) the introduction of an inner scale has virtually no effect, except at frequencies exceeding the spectral break.

A similar experiment to this was performed by *Vats et al*. [1981], who examined the effect of varying the inner scale wave number on the intensity variations. We, by contrast, impose the inner scale gradually by means of steepening high-frequency slope. In both cases, small-scale ionospheric structure is eroded and the efficacy of large-scale focusing is increased as a result. *Vats et al*. [1981] noted that the removal of small-scale structure via progressively increasing the inner scale (even all the way up to the Fresnel scale) does not appreciably alter the small-scale intensity variations if the scatter is sufficiently strong. This suggests that these small-scale intensity variations are indeed produced by large-scale features in the ionospheric structure. Indeed, the scintillations at all scales are dominated by the contribution from the large-scale structure. Cases of shallow sloped spectra exhibit a greater effect since more small-scale structure is initially present and able to be

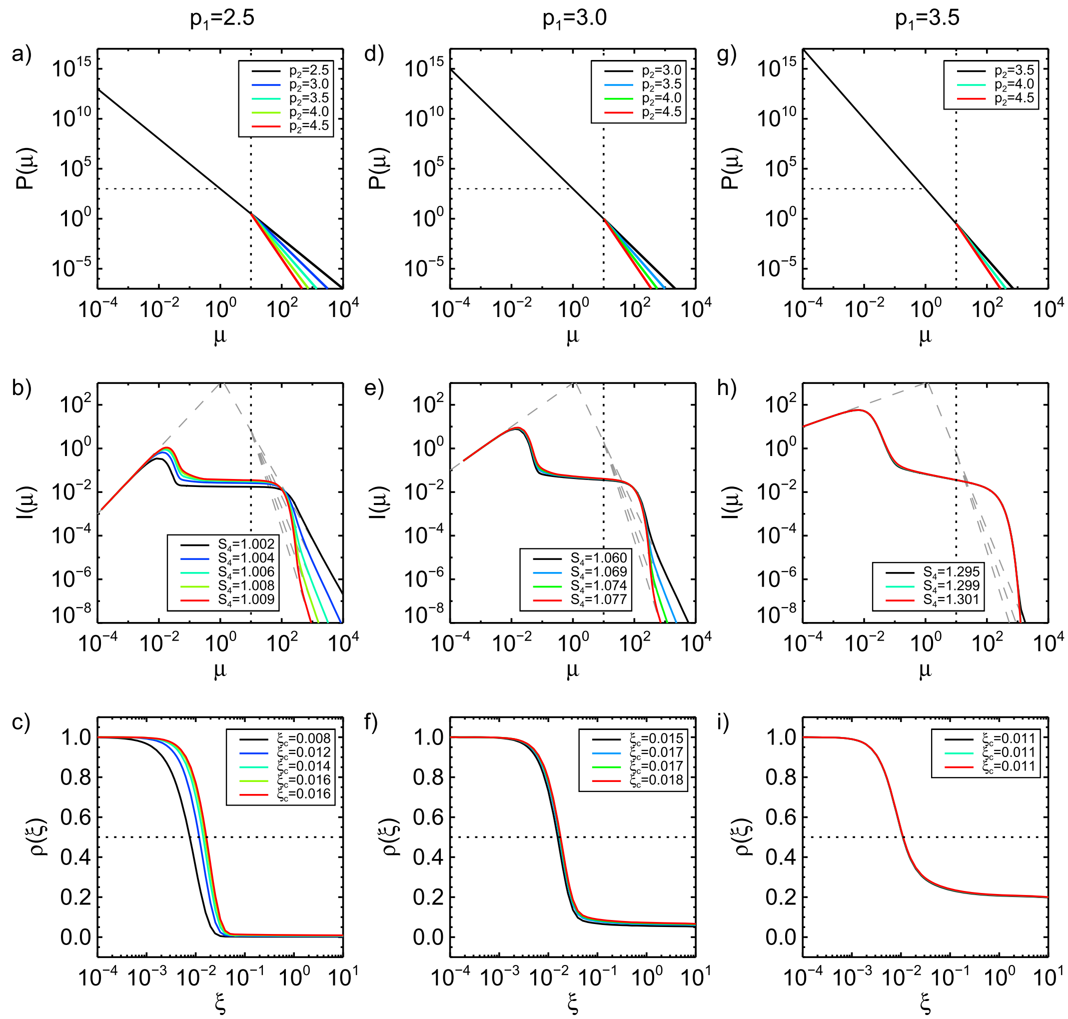

Figure 6. Effect of an inner spectral break at wave number $\mu_0 = 10$ under strong scatter conditions with $U = 1000$. The individual panels show the (a, d, and g) phase spectra, (b, e, and h) intensity spectra, and (c, f, and i) intensity correlation functions for different values of the high-frequency spectral index p_2 when the low-frequency spectral index is $p_1 = 2.5$ (Figures 6a–6c), $p_1 = 3.0$ (Figures 6d–6f), and $p_1 = 3.5$ (Figures 6g–6i).

suppressed than cases of steeply sloped spectra. Another important consequence of the inner scale is that it alters the shape of the intensity spectrum at asymptotically high frequencies. *Alimov and Rakhlin* [1996] noted that the absence of an inner scale leads to power law behavior at high frequencies rather than the Gaussian-like decay observed in *Booker and MajidiAhi*'s simulations [1981]. *Alimov and Rakhlin* [1996] as well as *Vats et al.* [1981] argued that for this reason the inclusion of an inner scale is important for reconciling the theory with multifrequency observations, particularly when the irregularity spectrum is shallow.

4.4. Morphologies of the Scintillation Index and Intensity Correlation Length

Next we examine the variation of the scintillation index and intensity correlation length as a function of the strength of scatter. Our purpose is to validate the theoretical predictions for S_4 and ξ_c previously presented in section 3 for the case of asymptotically strong scatter. Again, we consider the cases of an unmodified power law, a modified power law with an outer scale, and a modified power law with an inner scale. In the weak scatter domain ($U \ll 1$) we confirmed that our numerical simulations are in agreement with the weak scatter theory. We omit the details of this validation for space considerations. When the scatter is strong, our numerical results show that S_4 and ξ_c are sensitive to an inner scale (but not an outer scale) when the irregularity spectrum is shallow ($p < 3$), while the converse is true when the irregularity spectrum is steep ($p > 3$). The asymptotic results presented in section 3 state this more strongly: in the limit of asymptotically strong scatter,

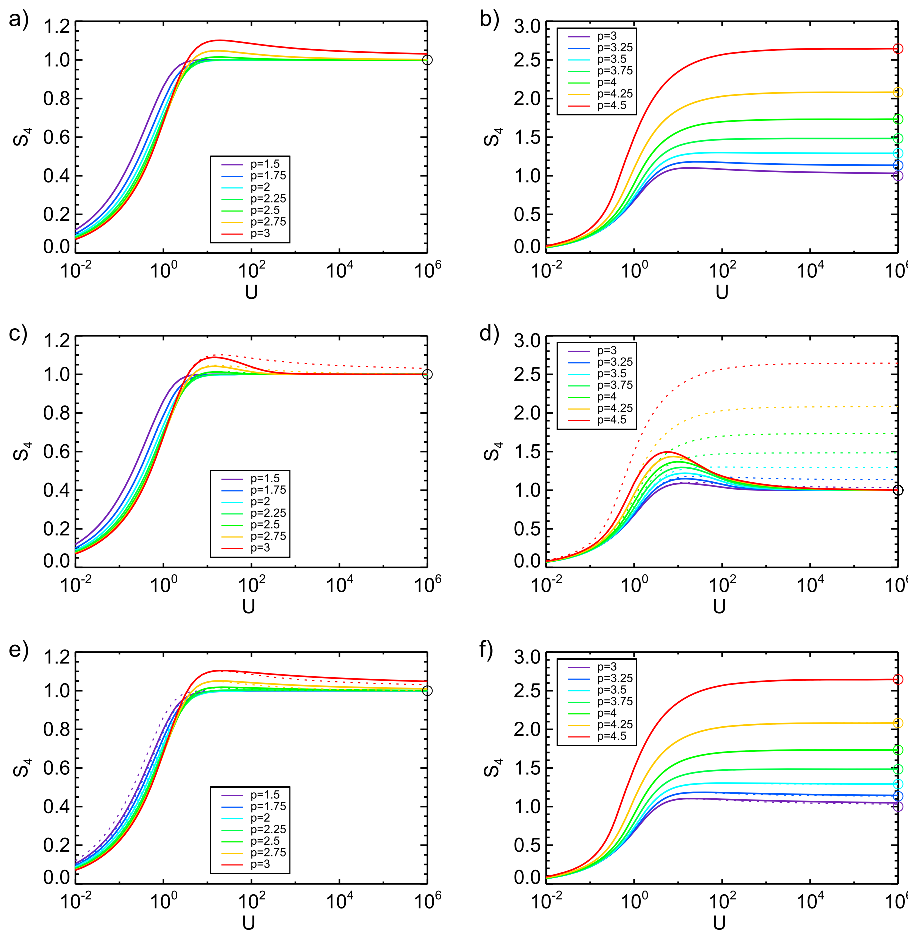

Figure 7. S_4 versus scattering strength U for different values of the phase spectral index ranging from (a, c, and e) 1.5 to 3.0 and from (b, d, and f) 3.0 to 4.5. The plots in Figures 7a and 7b correspond to an unmodified power law, Figures 7c and 7d to the outer scale case with $\mu_0 = 0.1$, and Figures 7e and 7f to the inner scale case with $\mu_0 = 10$. Open circles shown along the right axis indicate theoretical limiting S_4 values.

S_4 and ξ_c are controlled entirely by the high-frequency portion of the irregularity spectrum ($\mu > \mu_0$) when the spectrum is shallow ($p_1 \leq p_2 < 3$) and entirely by the low-frequency portion of the irregularity spectrum ($\mu < \mu_0$) when the spectrum is steep ($p_2 > p_1 > 3$). For the general case with $p_1 < 3$, $p_2 > 3$, irregularity scale sizes both smaller and larger than the Fresnel scale can contribute to the intensity statistics. In this case, the location of the spectral break relative to the Fresnel scale dictates the development of the intensity field.

Figure 7 compares the dependence of S_4 on the scattering strength for an unmodified power law (Figures 7a and 7b), a modified power law with an outer scale (Figures 7c and 7d), and a modified power law with an inner scale (Figures 7b, 7d, and 7f). The dashed curves show the S_4 for an unmodified power law to facilitate the comparison. First, consider the unmodified power law case (Figure 7a). When $p < 3$, the S_4 index saturates at unity (with overshoot if $p > 2$). The increase of S_4 with increasing U is monotonic if either $p \leq 2$ or $p \geq 4$. Power law spectra with $p > 3$ admit sustained quasi-saturation states with $S_4 > 1$. The open circles shown along the right axis indicate the theoretical limiting values given in (20). The agreement with theory is excellent, except for the case $p = 3$. The reason for this apparent discrepancy is that when $p = 3$ the S_4 index converges to unity from above extremely slowly (we confirmed this by increasing the scattering strength in logarithmic steps to $U = 10^{12}$). Next, consider the case when an outer scale has been imposed, Figure 7b). For shallow spectra ($p < 3$), the outer scale has only the minor effect of causing the saturation state $S_4 = 1$ to be approached more quickly as the scattering strength increases. For steep spectra ($p > 3$) the effect of the outer scale is much more dramatic. The suppression of large-scale irregularity structure mitigates the quasi-saturation state and causes S_4 to retreat from its maximum value with increasing perturbation strength, ultimately converging to unity from

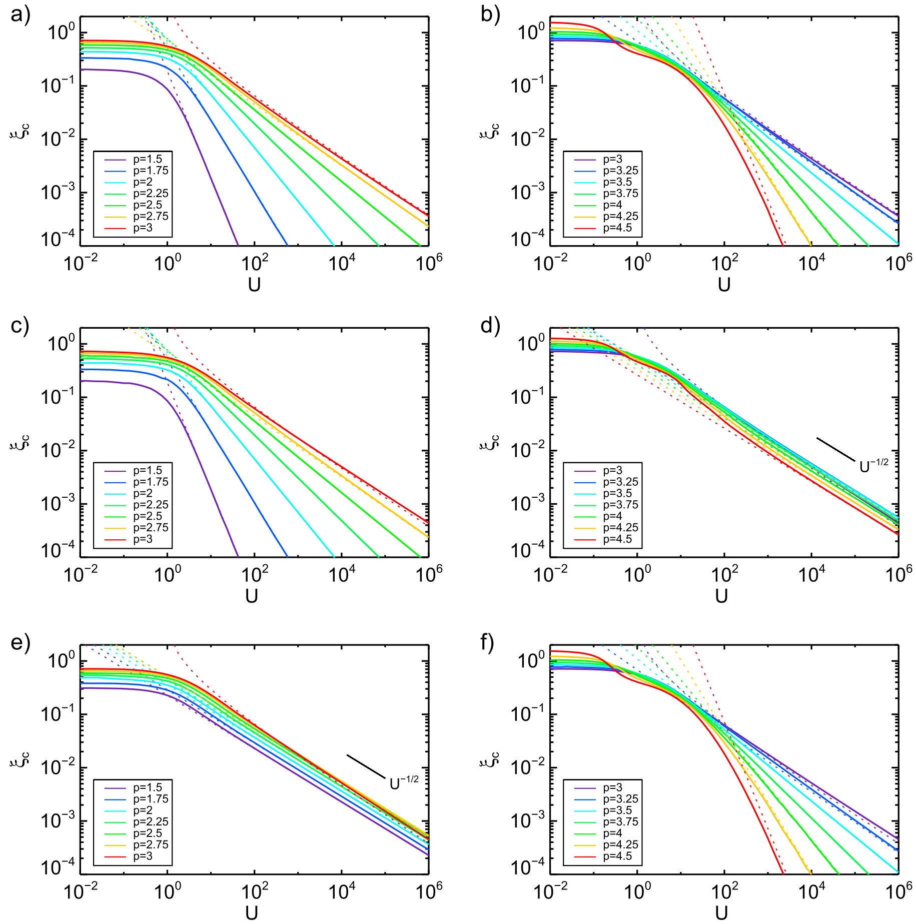

Figure 8. Intensity correlation length ξ_c versus scattering strength U for different values of the phase spectral index ranging from (a, c, and e) 1.5 to 3.0 and from (b, d, and f) 3.0 to 4.5. The plots in Figures 8a and 8b correspond to an unmodified power law, Figures 8c and 8d to the outer scale case with $\mu_0 = 0.1$, and Figures 8e and 8f to the inner scale case with $\mu_0 = 10$. Dotted lines indicate theoretical asymptotic ξ_c behavior.

above. From this we infer that strong focusing by large-scale structure is responsible for sustaining quasi-saturation states with $S_4 > 1$. A detailed discussion of quasi-saturation states with $S_4 > 1$ and how they are mitigated by the presence of an outer scale may be found in Chapter 7 of the book by *Jakeman and Ridley* [2006].

The scattering strength at which the maximum S_4 occurs is associated with peak focusing effects. Since U depends on the ionospheric perturbation strength, frequency, and distance to the screen, all of these effects are involved in determining the peak focusing condition for a given irregularity model. The maximum S_4 that can be achieved depends on the form of the irregularity model (defined by p_1, p_2, and μ_0). This maximum may be used to discriminate between prospective models used to interpret scintillation measurements. For instance, S_4 values well above unity cannot occur in conjunction with a shallow irregularity spectrum ($p < 3$). At least some portion of the spectrum near the Fresnel scale $\mu = 1$ must be steep for this to occur. Restated in physical terms, S_4 values well above unity cannot occur in the presence of significant small-scale structure, since this structure mitigates the efficacy of strong focusing by the large-scale irregularities.

Finally, we consider the case when an inner scale has been imposed (Figure 7c). For shallow irregularity spectra ($p < 3$), the presence of an inner scale tends to increase S_4 throughout the weak scatter regime relative to the unmodified power law case. The effect is relatively minor except when the irregularity spectrum is very shallow. For moderately sloped spectra ($p \approx 3$) the introduction of an inner scale mitigates some of the strong focusing effect, but this effect is also minor. For steeply sloped spectra ($p > 3$) the inner scale has essentially no effect on the development of S_4.

Figure 8 compares the dependence of intensity correlation length on the scattering strength for an unmodified power law (Figures 8a and 8b), a modified power law with an outer scale (Figures 8c and 8d), and a modified power law with an inner scale (Figures 8b, 8d, and 8f). The dotted lines show the theoretical limiting correlation length. First, consider the case for an unmodified power law (Figure 8a). When $p < 3$, the theoretical correlation length is that given by (21). The intensity correlation length is an excellent diagnostic of the presence of small-scale variations in the intensity field. The abundance of small-scale intensity structure generated through diffractive processes produces a rapidly decreasing correlation length with $\xi_c \propto U^{-1/(p-1)}$. For the cases with $p > 3$ the theoretical correlation length is that given in (24) and (25). In this case, the small-scale intensity variations are generated by strong focusing by the large-scale structure, which also results in a rapidly decreasing correlation length with $\xi_c \propto U^{-1/(5-p)}$. In both cases, the agreement between the simulation and the theoretical results is excellent when U is sufficiently large. Figure 8b shows the dependence of the intensity correlation length on the scattering strength when an outer scale is present ($p_1 = 0$, $\mu_0 = 0.1$). For shallow spectra ($p_2 < 3$), the correlation length is practically unaffected by the presence of the outer scale. The theoretical result (21) is in excellent agreement with the simulations when U is sufficiently large. For steep spectra ($p_2 > 3$), the outer scale mitigates the production of small-scale intensity fluctuations via strong focusing which leads to a significantly slower rate of decrease in the correlation length $\xi_c \propto U^{-1/2}$. The theoretical result (26) is in excellent agreement with the simulation results for large U. Finally, consider the case when an inner scale is imposed ($p_2 = 4.5$, $\mu_0 = 10$) (Figure 8c). In this case, we find that the correlation length is affected for shallow spectra ($p_1 < 3$) and the theoretical result (26) is in excellent agreement with the simulation results for large U. For steep spectra ($p_1 > 3$) the results resemble those of the unmodified power law case and the theoretical results (24) and (25) are in excellent agreement with the simulations for large U. We note that the correlation length for the moderately sloped case $p = 3$ is relatively insensitive to the presence of either an outer scale or inner scale.

4.5. The Transition From One- to Two-Component Power Law Behavior

In the previous section, we validated the theoretical predictions for S_4 and ξ_c that were given in section 3 for the case of asymptotically strong scatter. In this section, we examine more closely the process by which this asymptotic state is attained as the scattering strength increases. A general spectral break is considered, which may occur at intermediate scales. Initially, let us assume that this spectral break is well separated from the Fresnel frequency (i.e., $\mu_0 \ll 1$ or $\mu_0 \gg 1$). In this case, as the strength of scatter U increases from weak to strong scatter, S_4 and ξ_c initially follow the same behavior as an unmodified power law with the dominant spectral index (the same index p as the segment containing the Fresnel scale), as if the spectral break was not present. This is not surprising since when the scatter is weak only those scale sizes in the irregularity structure close to the Fresnel scale contribute to the intensity variations. As the scattering strength increases so does the range of spatial scales in the irregularity structure that contributes to the intensity variations. When the scatter becomes sufficiently strong, irregularity scales on both sides of the spectral break contribute to the intensity statistics. When this occurs, the development transitions to that for a two-component power law (which is unique from the development for an unmodified power law of either slope). In essence, the intensity statistics do not show the effect of the spectral break until the scattering is sufficiently strong for the break to be felt. *Uscinski et al.* [1981] came to a similar conclusion by noting that the presence of an outer scale does not affect the intensity statistics if the observer is sufficiently close to the screen. Exploiting the universal scaling, we can generalize this notion from distance to the screen to scattering strength U, which depends on irregularity strength, frequency, and distance to the screen in a particular way. Below we present quantitative guidelines for predicting whether a general spectral break will be felt or not and hence whether the asymptotic results for the unmodified or two-component models will more accurately reflect the results of an experiment for a given strength of scatter. This idea is conveyed most easily using examples.

Figure 9 shows the development of S_4 (Figures 9a–9c) and intensity correlation length ξ_c (Figures 9d–9f) versus scattering strength U. Three cases are shown for comparison: an unmodified power law with $p = 2$ (blue), a two-component power law with $p_1 = 2$ and $p_2 = 4$ (purple), and an unmodified power law with $p = 4$ (red). Figures 9a and 9d correspond to $\mu_0 = 0.01$, Figures 9b and 9e to $\mu_0 = 1$, and Figures 9c and 9f to $\mu_0 = 100$. Open circles shown along the right axis indicate theoretical limiting S_4 values. Dashed lines indicate theoretical asymptotic ξ_c behavior.

First, consider the case of an outer scale well separated from the Fresnel scale (Figures 9a and 9d). The Fresnel scale lies in the high-frequency portion of the irregularity spectrum. Because of this, at small values of U the

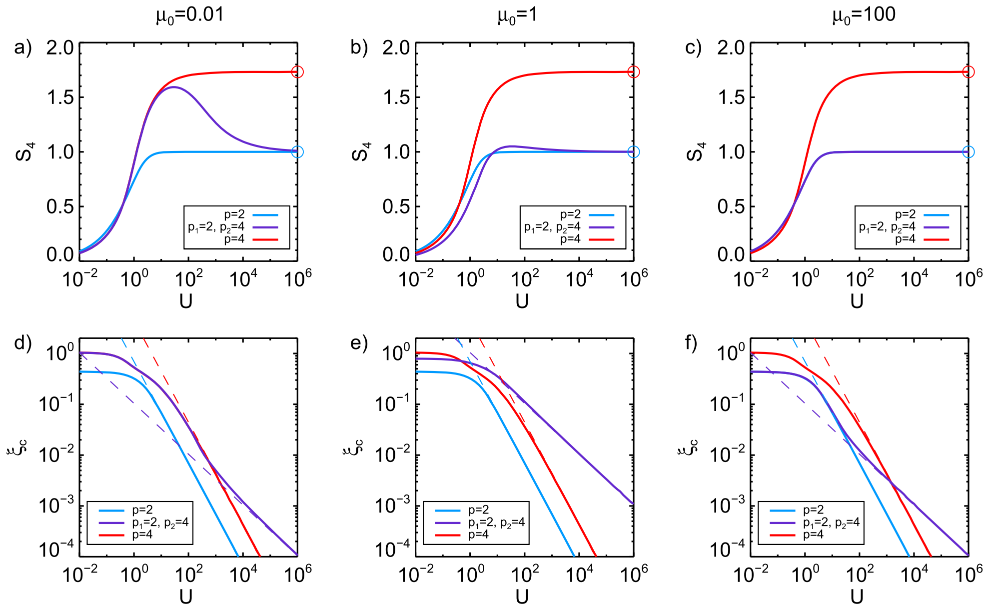

Figure 9. (a–c) S_4 index and (d–f) intensity correlation length ξ_c versus scattering strength U. Three cases are shown for comparison: an unmodified power law with $p = 2$ (blue), a two-component power law with $p_1 = 2$ and $p_2 = 4$ (purple), and an unmodified power law with $p = 4$ (red). Figures 9a and 9d correspond to $\mu_0 = 0.01$, Figures 9b and 9e to $\mu_0 = 1$, and Figures 9c and 9f to $\mu_0 = 100$. Open circles shown along the right axis indicate theoretical limiting S_4 values. Dashed lines indicate theoretical asymptotic ξ_c behavior.

development of S_4 and ξ_c resembles that for an unmodified power law with spectral index $p = 4$ (shown in red, for comparison). Since this spectrum is steep, strong focusing leads to S_4 values in excess of 1.5 and the generation of small-scale intensity structure via large-scale focusing produces a rapidly decreasing correlation length with $\xi_c \propto U^{-1}$. As the scattering strength increases so does the range of spatial scales in the irregularity structure that contributes appreciably to the integral (11). At small to intermediate values of U this contribution comes predominantly from the steep high-frequency portion of the irregularity spectrum with $p_2 = 4$, but as the strength of scatter increases, eventually, there is also a contribution from the shallow low-frequency portion with $p_1 = 2$. At this point, the development transitions to follow that uniquely characteristic of a two-component spectrum with $p_1 = 2$ and $p_2 = 4$ for further increases in U. Specifically, as the strength of scatter increases further, S_4 retreats from its local maximum and decreases toward unity, while the intensity correlation length decreases at the slower rate, $\xi_c \propto U^{-1/2}$. Note that this transition occurs close to the value of U at which the asymptotic ξ_c curve (21) for an unmodified power law with $p = 2$ (blue dashed curve) intersects the asymptotic ξ_c curve (26) for a two-component spectrum with $p_1 = 2$ and $p_2 = 4$ (purple dashed curve). From the scattering strength at which this intersection occurs, the definition of U, equations (10) and (16), and given the ionospheric perturbation strength C'_p and frequency $f = k/2\pi$, we can compute the distance from the screen at which the spectral break is first felt in the sense that there is a detectable response to the break in the intensity statistics.

Next, consider the case of an inner scale well separated from the Fresnel scale (Figures 9c and 9f). The Fresnel scale now lies in the low-frequency portion of the irregularity spectrum. Because of this, at small values of U the development of S_4 and ξ_c resembles that for an unmodified power law with spectral index $p = 2$ (shown in blue, for comparison). Since this spectrum is shallow, strong focusing is ineffective and S_4 undergoes a monotonic approach toward unity, while the abundance of small-scale intensity structure generated through diffractive processes produces a rapidly decreasing correlation length with $\xi_c \propto U^{-1}$. At small to intermediate U the contribution to the integral (11) comes predominantly from the shallow low-frequency portion of the irregularity spectrum with $p_1 = 2$, but as the strength of scatter increases eventually there is also a contribution from the steep high-frequency portion with $p_1 = 4$. At this point, the development transitions to follow that characteristic of a two-component spectrum with $p_1 = 2$ and $p_2 = 4$ for further increases in U. The S_4 index continues its trajectory toward unity, while the intensity correlation length decreases at the slower rate, $\xi_c \propto U^{-1/2}$. Note that this

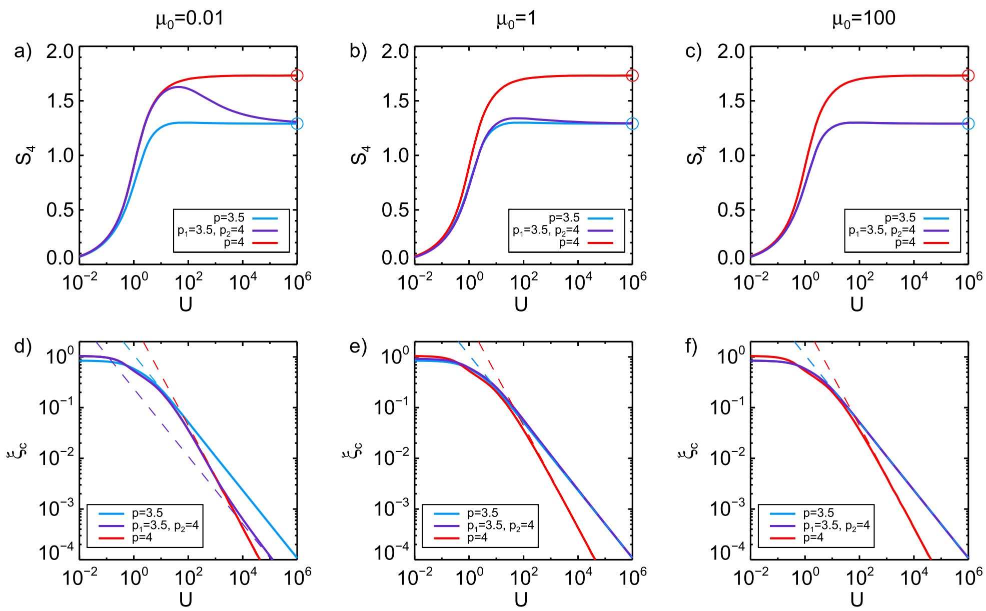

Figure 10. (a–c) S_4 index and (d–f) intensity correlation length ξ_c versus scattering strength U. Three cases are shown for comparison: an unmodified power law with $p = 3.5$ (blue), a two-component power law with $p_1 = 3.5, p_2 = 4$ (purple), and an unmodified power law with $p = 4$ (red). Figures 10a and 10d correspond to $\mu_0 = 0.01$, Figures 10b and 10e to $\mu_0 = 1$, and Figures 10c and 10f to $\mu_0 = 100$. Open circles shown along the right axis indicate theoretical limiting S_4 values. Dashed lines indicate theoretical asymptotic ξ_c behavior.

transition occurs close to the value of U at which the asymptotic ξ_c curve (24) for an unmodified power law with $p = 4$ (red dashed curve) intersects the asymptotic ξ_c curve (26) for a two-component spectrum with $p_1 = 2$ and $p_2 = 4$ (purple dashed curve). As before, the scattering strength at which this intersection occurs can be used with equations (10) and (16), along with the ionospheric perturbations strength C_p' and frequency to compute the distance from the screen at which the spectral break first influences the intensity statistics.

Finally, consider the case of a spectral break that is close (or, in this case, equal) to the Fresnel wave number (Figures 9b and 9e). In this case the contribution to the integral (11) comes from both sides of the spectral break, even when the scatter is weak. In this case, the presence of the break is detectable at any strength of scatter and the development of S_4 and ξ_c will be that of a two-component spectrum (which is unique from the development for an unmodified power law of either slope). In this case, as the scatter becomes strong there is a small overshoot in the approach of S_4 toward unity which was absent from the inner scale case (Figure 9c). This overshoot is due to the increased efficacy of large-scale focusing as a result of the suppression of small-scale structure relative to the inner scale case. As soon as the intensity correlation length begins to vary with increasing strength of scatter, the rate of decrease is the slower rate predicted for a two-component power law, $\xi_c \propto U^{-1/2}$.

We repeated this experiment using a different value of the low-frequency irregularity slope in order to demonstrate the establishment of a quasi-saturation state for two-component irregularity spectra with $p_2 > p_1 > 3$. Figure 10 shows the development of S_4 (Figures 10a–10c) and intensity correlation length ξ_c (Figures 10d–10f) versus scattering strength U. The following three cases are shown for comparison: an unmodified power law with $p = 3.5$ (blue), a two-component power law with $p_1 = 3.5$ and $p_2 = 4$ (purple), and an unmodified power law with $p = 4$ (red). Figures 10a and 10d correspond to $\mu_0 = 0.01$, Figures 10b and 10e to $\mu_0 = 1$, and Figures 10c and 10f to $\mu_0 = 100$. Open circles shown along the right axis indicate theoretical limiting S_4 values. Dashed lines indicate theoretical asymptotic ξ_c behavior. Note that the limiting value of S_4 is significantly higher than unity for all curves in Figure 10. The asymptotic theoretical result (20) predicts that the limiting S_4 will be $(5/3)^{1/2}$ for both the unmodified power law with $p = 3.5$ (blue curve) and the two-component power law with $p_1 = 3.5$ and $p_2 = 4$ (purple). Similarly, the theoretical result (20) predicts that the limiting S_4 will be $(3)^{1/2}$ for the unmodified power law with $p = 4$ (red). These predictions are well substantiated by the results of the numerical simulation shown in Figure 10. The slight change in index between p_1 and p_2 is not sufficient to mitigate the development of small-scale structure via strong focusing in this case. As in the previous case (Figure 9), when the spectral break is well separated from the Fresnel scale (Figures 9a and 9c), the development of S_4 and ξ_c initially (low to moderate U) follows the asymptotic behavior of an unmodified power law with the dominant spectral index. At the value of U where the asymptotic ξ_c curves for this unmodified power law and the two-component law intersect, the development transitions to that predicted for the latter. We note that for the outer scale case (Figure 9a) this transition takes place very slowly (over several orders of magnitude in scattering strength). We also note that the development is relatively similar for the cases with $\mu_0 = 1$ and $\mu_0 = 0.01$. The reason for this is that the change in index at the spectral break from $p_1 = 3.5$ to $p_2 = 4.0$ is relatively small in this case.

5. Conclusions

In this paper we have extended the power law phase screen theory for ionospheric scintillation to account for the case where the refractive index irregularities follow a two-component power law spectrum. Using this spectral model, we solved the fourth moment equation governing the intensity fluctuations for the case of two-dimensional field-aligned ionospheric irregularities. A specific normalization was invoked to exploit the self-similar properties of the problem to achieve a universal scaling, such that different combinations of perturbation strength, propagation distance, and frequency produce the same results. The numerical algorithm was validated using new theoretical predictions for the behavior of the scintillation index and intensity correlation length under strong scatter conditions. A number of numerical experiments were performed to explore the morphologies of the intensity spectrum, scintillation index, and intensity correlation length as functions of the spectral indices and strength of scatter; retrieve phase screen parameters from intensity scintillation observations; investigate the effects of an imposed outer scale, intermediate break scale, or inner scale on the development of the scintillation; explore the relative contributions to scintillation due to large- and small-scale ionospheric structures; and quantify the conditions under which a general spectral break will influence the scintillation statistics.

Our first conclusions are relevant to the behavior of the intensity statistics in the strong scatter regime. The asymptotic results presented in section 3 show that for shallow spectra ($p_1 \le p_2 < 3$) the limiting behavior of the intensity statistics is dictated by the high-frequency portion of the irregularity spectrum ($\mu > \mu_0$), whereas for steep spectra ($p_2 > p_1 > 3$) it is dictated by the low-frequency portion of the irregularity spectrum ($\mu < \mu_0$). Our numerical results confirm that shallow power law spectra are sensitive to an inner scale but insensitive to an outer scale; conversely steep spectra are sensitive to an outer scale but insensitive to an inner scale. Unmodified power law spectra with $p \approx 3$ are relatively insensitive to both outer and inner scales. We note that the two-component model allows for only one spectral break, and therefore, we cannot impose both outer and inner scales simultaneously. It turns out that this restriction is not limiting in practice because only one of these exerts controls on the scintillation statistics at a time. An outer scale can be omitted from the model without consequence if the spectrum is shallow; similarly, an inner scale can be omitted from the model without consequence if the spectrum is steep. For mixed-slope spectra ($p_1 < 3$, $p_2 > 3$), irregularity scales both large and small contribute to the intensity statistics in the strong scatter limit. In this case, the spectral slopes and location of the spectral break relative to the Fresnel scale control the development of the intensity statistics. It should be noted, however, that the irregularities must be homogenous for the statistical theory of scintillation to be valid (i.e., the structure must admit Fourier decomposition). If the irregularities are inhomogeneous at the largest scale sizes, an outer scale may not be clearly defined. Departures from the strong scatter theory may be anticipated if the large-scale inhomogeneous structures play a dominant role in the scattering.

By manipulating the large- or small-frequency spectral slopes in the two-component model, we gradually eroded large- and small-scale irregularity structures and observed the effects on scintillation development in the strong scatter regime. Steep power law irregularity spectra emphasize the large-scale structures which generate small-scale irregularity structure via strong focusing. Shallow power law irregularity spectra emphasize the small-scale irregularity structures which scatter the radio waves more effectively (in a wider range of directions), thereby reducing the efficacy of large-scale focusing. For shallow irregularity spectra, the small-scale intensity variations are generated primarily by small-scale irregularity structures via diffraction. The shape of the irregularity spectrum determines the relative proportion of these two classes of ionospheric structure, and therefore which of these physical processes (focusing vs. diffraction) will exert a dominant role, the slope $p = 3$ being the special case in which these physical processes are in relative balance. In our numerical experiments, we observed that if the spectrum is steep ($p < 3$), eroding the large-scale structure suppresses both the low-frequency enhancement and high-frequency spectral broadening. Hence, the large-scale irregularity structure is responsible for generating (via focusing) these intensity variations at the large and small scales. If the spectrum is shallow ($p < 3$), eroding the small-scale structure suppresses the small-scale intensity variations. Hence, the small-scale irregularity structure is responsible for generating (via diffraction) the small-scale intensity variations. Interestingly, the erosion of small-scale structure also promotes focusing by the larger-scale structure that remains. This focusing acts to increase the power in the intensity fluctuations at all scales between the low-frequency return to power law and the spectral break. In particular, the low-frequency enhancement grows in amplitude as the small-scale structure is progressively eroded. This behavior demonstrates the highly nonlocal behavior in frequency, which is caused by the nonlinearity of the system, when the scatter is strong. This is in stark contrast to the weak scatter case, where each scale size of the intensity fluctuations is controlled by the corresponding scale size in the structure.

Previous researchers have observed that the presence of small-scale structure associated with fully developed plasma turbulence at low latitudes in the early postsunset hours tends to suppress strong focusing and inhibit S_4 values exceeding unity [*Bhattacharyya et al.*, 1992, 2003; *Engavale and Bhattacharyya*, 2005]. Later in the evening, diffusive processes erode the small-scale structure, which encourages strong focusing and can result in S_4 values well above unity. *Engavale and Bhattacharyya* [2005] noted that "large-scale irregularities give rise to focusing effects ($S_4 > 1$) when phase fluctuations are sufficiently large. The focusing effect is absent for irregularities with power law spectra that have shallow slopes ($p < 3$), which implies a significant presence of small-scale irregularities." These authors also considered the two-component spectrum with $p_1 = 2$, $p_2 = 4$, which we classify as mixed-slope type. They noted that "the break frequency must be sufficiently large ($\mu_0 < 1$) in order for S_4 to exhibit focusing effects; otherwise, the small-scale irregularities are effective in scattering the radio waves and the focusing effect is lost." Our results are consistent with these earlier observations.

We also conducted numerical experiments to investigate the process by which the asymptotic state is attained as the scattering strength is increased. First, consider the situation where the spectral break is well separated from the Fresnel frequency. As the strong scatter regime is approached the scintillation index and correlation length initially follow the behavior for an unmodified power law with the dominant spectral index. Effectively, the intensity field develops as if the spectral break was not present. This is not surprising since when the scatter is weak only those scales in the irregularity structure close to the Fresnel scale contribute to the intensity variations. As the scattering strength increases so does the range of spatial scales in the irregularity structure that contributes to the intensity variations. When the scatter becomes sufficiently strong, irregularity scales on both sides of the spectral break contribute to the intensity statistics. When this occurs, the development of the scintillation index and correlation length undergoes a transition to follow the behavior for a two-component spectrum. This behavior differs from the development for an unmodified power law of either slope. When the spectral break is not well separated from the Fresnel frequency, irregularity scales on both sides of the spectral break contribute to the intensity statistics even in weak scatter. In this case, the intensity statistics reflect the presence of the break at any strength of scatter and the development of the scintillation index and correlation length follows the behavior unique to a two-component spectrum. In summary, depending on the scale separation between the spectral break and Fresnel frequency, the intensity statistics do not "feel" the break until the scattering is sufficiently strong. We show that the transitional strength of scatter at which the spectral break begins to be felt occurs near the intersection of the asymptotic correlation lengths predicted for the unmodified and two-component power law models.

Uscinski et al. [1981] came to a similar conclusion by noting that the presence of an outer scale does not affect the intensity statistics if the observer is sufficiently close to the screen. The results of our analysis generalize this notion to the case of an arbitrarily located spectral break. Moreover, by exploiting the universal scaling we can generalize the Uscinski result for any combination of irregularity strength, frequency, and distance to the screen. We are therefore able to predict whether a general spectral break will be felt or not and thus whether the asymptotic results for the unmodified or two-component power law models will more accurately reflect the results of an experiment. This has important ramifications for applications which use measurements of the intensity correlation length to infer the strength of scintillation when the observations are saturated [*Franke and Liu*, 1983; *Carrano et al.*, 2015].

Acknowledgments

The authors would like to acknowledge partial financial support from the Air Force Research Laboratory contracts FA87-18-09-C-0041 and FA9453-12-C-0239. The intensity scintillation data from Ascension Island (Figure 4) were provided by the Air Force Research Laboratory. Requests for this data should be addressed to Ronald Caton (ronald.caton.1@us.af.mil) or Todd Pedersen (todd.pedersen@us.af.mil).

References

Alimov, V. A., and A. V. Rakhlin (1996), Amplitude fluctuations in the theory of radio-wave refraction scattering, *Radiophys. Quantum Electron.*, *39*(9), 744–751.

Basu, S., S. Basu, J. P. McClure, W. B. Hanson, and H. E. Whitney (1983), High resolution topside in situ data of electron densities and VHF/GHz scintillations in the equatorial region, *J. Geophys. Res.*, *88*(A1), 403–415, doi:10.1029/JA088iA01p00403.

Bhattacharyya, A., and K. C. Yeh (1988), Intensity correlation function for waves of different frequencies propagating through a random medium, *Radio Sci.*, *23*(5), 791–808, doi:10.1029/RS023i005p00791.

Bhattacharyya, A., K. C. Yeh, and S. J. Franke (1992), Deducing turbulence parameters from transionospheric scintillation measurements, *Space Sci. Rev.*, *61*(3-4), 335–386.

Bhattacharyya, A., K. M. Groves, S. Basu, H. Kuenzler, C. E. Valladares, and R. Sheehan (2003), L-band scintillation activity and space-time structure of low-latitude UHF scintillations, *Radio Sci.*, *38*(1), 1004, doi:10.1029/2002RS002711.

Booker, H., and G. MajidiAhi (1981), Theory of refractive scattering in scintillation phenomena, *J. Atmos. Sol. Terr. Phys.*, *43*, 1199–1204.

Booker, H. G., J. A. Ratcliffe, and D. H. Shinn (1950), Diffraction from an irregular screen with applications to ionospheric problems, *Philos. Trans. R. Soc. London Ser. A.*, *242*, 579–607.

Carrano, C. S., C. E. Valladares, and K. M. Groves (2012), Latitudinal and local time variation of ionospheric turbulence parameters during the Conjugate Point Equatorial Experiment in Brazil, *Int. J. Geophys.*, *2012*, 103963, doi:10.1155/2012/103963.

Carrano, C. S., K. M. Groves, S. H. Delay, and P. H. Doherty (2015), On the mutual coherence function for transionospheric waves and its utility for characterizing ionospheric irregularities with a GNSS Scintillation Monitor, Proceedings of the 2015 ION Pacific PNT Conference, Honolulu, Hawaii, 20–23 April.

Engavale, B., and A. Bhattacharyya (2005), Spatial correlation function of intensity variations in the ground scintillation pattern produced by equatorial spread-F irregularities, *Indian J. Radio Space Phys.*, *34*, 23–32.

Forte, B. (2008), Refractive scattering evidence from multifrequency scintillation spectra observed at auroral latitudes, *Radio Sci.*, *43*, RS2012, doi:10.1029/2007RS003715.

Forte, B. (2012), Analysis of strong ionospheric scintillation events measured by means of GPS signals at low latitudes during disturbed conditions, *Radio Sci.*, *47*, RS4009, doi:10.1029/2011RS004789.

Franke, S. J., and C. H. Liu (1983), Observations and modeling of multi-frequency VHF and GHz scintillations in the equatorial region, *J. Geophys. Res.*, *88*(A9), 7075–7085, doi:10.1029/JA088iA09p07075.

Franke, S. J., and C. H. Liu (1985), Modeling of equatorial multifrequency scintillation, *Radio Sci.*, *20*(3), 403–415, doi:10.1029/RS020i003p00403.

Gherm, V. E., and N. N. Zernov (2015), Strong scintillation of GNSS signals in inhomogeneous ionosphere: 2. Computer simulator of random signals, *Radio Sci.*, *50*, 168–176, doi:10.1002/2014RS005604.

Gochelashvily, K. S., and V. I. Shishov (1971), Laser beam scintillation beyond a turbulent layer, *Opt. Acta*, *18*(4), 313–320.

Gozani, J. (1985), Numerical solution of the fourth order coherence function of a plane wave propagating in a two-dimensional Kolmogorovian medium, *J. Opt. Soc. Am.*, *A12*, 2144–51.

Hewish, A. (1951), The diffraction of radio waves in passing through a phase-changing ionosphere, *Proc. R. Soc. London Ser. A.*, *209*, 81–96.

Hewish, A. (1989), A user's guide to scintillation, *J. Atmos. Terr. Phys.*, *51*(9/10), 743–750.

Ishimaru, A. (1997), *Wave Propagation and Scattering in Random Media*, IEEE Press and Oxford Univ., New York.

Jakeman, E., and K. D. Ridley (2006), *Modeling Fluctuations in Scattered Fields*, CRC Press, Taylor and Francis, Boca Raton, Fla.

Johansson, F., et al. (2013), Mpmath: A Python library for arbitrary-precision floating-point arithmetic (version 0.18), December 2013. [Available at http://mpmath.org/.]

Mercier, R. P. (1962), Diffraction by a screen causing large random phase fluctuations, *Proc. Cambr. Phil. Soc.*, *58*, 382, doi:10.1017/S0305004100036586.

Ooura, T., and M. Mori (1991), The double exponential formula for oscillatory functions over the half infinite interval, *J. Comput. Appl. Math.*, *38*, 353–360.

Rino, C. (1979a), A power law phase screen model for ionospheric scintillation: 1. Weak scatter, *Radio Sci.*, *14*, 1135–1145, doi:10.1029/RS014i006p01135.

Rino, C. L. (1979b), A power law phase screen model for ionospheric scintillation: 2. Strong scatter, *Radio Sci.*, *14*(6), 1147–1155, doi:10.1029/RS014i006p01135.

Rino, C. L. (1980), Numerical computations for a one-dimensional power law phase screen, *Radio Sci.*, *15*(1), 41–47, doi:10.1029/RS015i001p00041.

Rino, C. L. (1982), On the application of phase screen models to the interpretation of ionospheric scintillation data, *Radio Sci.*, *17*(4), 855–867, doi:10.1029/RS017i004p00855.

Rino, C. L. (2011), *The Theory of Scintillation With Applications in Remote Sensing*, John Wiley, New York.

Rino, C. L., and C. S. Carrano (2013), A compact strong-scatter scintillation model: Proceedings of the International Beacon Satellite Symposium, Bath, U. K., 8–12 July.

Rino, C. L., and J. Owen (1984), Numerical simulations of intensity scintillation using the power law phase screen model, *Radio Sci.*, *19*(3), 891–908, doi:10.1029/RS019i003p00891.

Rino, C. L., C. S. Carrano, and P. Roddy (2014), Wavelet-based analysis and power law classification of C/NOFS high-resolution electron density data, *Radio Sci.*, *49*, 680–688, doi:10.1002/2013RS005272.

Rino, C. L., C. S. Carrano, K. M. Groves, and P. A. Roddy (2016), A characterization of intermediate-scale spread-*F* structure from four years of high-resolution C/NOFS satellite data, *Radio Sci.*, *51*, doi:10.1002/2015RS005841.

Rufenach, C. L. (1974), Wavelength dependence of radio scintillation: Ionosphere and interplanetary irregularities, *J. Geophys. Res.*, *79*(10), 1562–1566, doi:10.1029/JA079i010p01562.

Rumsey, V. H. (1975), Scintillation due to a concentrated layer with a power-law turbulence spectrum, *Radio Sci.*, *10*(1), 107–114, doi:10.1029/RS010i001p00107.

Salpeter, E. E. (1967), Interplanetary scintillations: I. Theory, *Astrophys. J.*, *147*, 433–448.

Shishov, I. (1974), Dependence of the form of the scintillation spectrum on the form of the spectrum of refractive index inhomogeneities: I. Phase screen, *Radiophys. Quantum Electron.*, *17*(11), 1287–1292.

Shishov, I. (1976), Scintillation spectrum as a function of the spectrum of refractive-index irregularities: II. Statistically homogeneous medium, *Radiophys. Quantum Electron.*, *19*, 62.

Singleton, D. G. (1970), Saturation and focusing effects in radio-star and satellite scintillations, *J. Atmos. Terr. Phys.*, *32*, 187–208.

Uscinski, B. J., H. G. Booker, and M. Marians (1981), Intensity fluctuations due to a deep phase screen with a power-law spectrum, *Proc. R. Soc. London Series A*, *374*(1759), 503–530.

Vats, H. O., H. G. Booker, and G. MajidiAhi (1981), Quantitative explanation of strong multi-frequency intensity scintillation spectra using refractive scattering, *J. Atmos. Sol. Terr. Phys.*, *43*(12), 1235–1241.

Welch, P. D. (1967), The use of fast Fourier transform for the estimation of power spectra: A method based on time averaging over short, modified periodograms, *IEEE Trans. Audio Electroacoust.*, *15*(2), 70–73.

Yeh, K. C., and C. H. Liu (1982), Radio wave scintillations in the ionosphere, *Proc. IEEE*, *70*, 324–360.

Zernov, N. N., and V. E. Gherm (2015), Strong scintillation of GNSS signals in the inhomogeneous ionosphere: 1. Theoretical background, *Radio Sci.*, *50*, 153–167, doi:10.1002/2014RS005603.